

1 **Tropospheric thermal forcing of the stratosphere through quasi-balanced**
2 **dynamics**

3 Jonathan Lin^{a,c} Kerry Emanuel,^b

4 ^a *Lamont-Doherty Earth Observatory, Columbia University, New York, New York*

5 ^b *Lorenz Center, Department of Earth, Atmospheric, and Planetary Sciences,
6 Massachusetts Institute of Technology, Cambridge, Massachusetts*

7 ^c *Department of Earth and Atmospheric Sciences, Cornell University, Ithaca, New York*

8 *Corresponding author:* Jonathan Lin, jlin@ldeo.columbia.edu

9 ABSTRACT: The steady response of the stratosphere to tropospheric thermal forcing via an SST
10 perturbation is considered in two separate theoretical models. It is first shown that an SST anomaly
11 imposes a geopotential anomaly at the tropopause. Solutions to the linearized quasi-geostrophic
12 potential vorticity equations are then used to show that the vertical length scale of a tropopause
13 geopotential anomaly is initially shallow, but significantly increased by diabatic heating from
14 radiative relaxation. This process is a quasi-balanced response of the stratosphere to tropospheric
15 forcing. A previously developed, coupled troposphere-stratosphere model is then introduced and
16 modified. Solutions under steady, zonally-symmetric SST forcing in the linear β -plane model show
17 that the upwards stratospheric penetration of the corresponding tropopause geopotential anomaly
18 is controlled by two non-dimensional parameters, (1) a dynamical aspect ratio, and (2) a ratio
19 between tropospheric and stratospheric drag. The meridional scale of the SST anomaly, radiative
20 relaxation rate, and wave-drag all significantly modulate these non-dimensional parameters. Under
21 Earth-like estimates of the non-dimensional parameters, the theoretical model predicts stratospheric
22 temperature anomalies 2-3 larger in magnitude than that in the boundary layer, approximately in
23 line with observational data. Using reanalysis data, the spatial variability of temperature anomalies
24 in the troposphere is shown to have remarkable coherence with that of the lower-stratosphere,
25 which further supports the existence of a quasi-balanced response of the stratosphere to SST
26 forcing. These findings suggest that besides mechanical and radiative forcing, there is a third way
27 the stratosphere can be forced – through the tropopause via tropospheric thermal forcing.

28 SIGNIFICANCE STATEMENT: Upwards motion in the tropical stratosphere, the layer of at-
29 mosphere above where most weather occurs, is thought to be controlled by weather disturbances
30 that propagate upwards and dissipate in the stratosphere. The strength of this upwards motion is
31 important since it sets the global distribution of ozone. We formulate and use simple mathematical
32 models to show the vertical motion in the stratosphere can also depend on the warming in the
33 troposphere, the layer of atmosphere where humans live. We use the theory as an explanation
34 for our observations of inverse correlations between the ocean temperature and the stratosphere
35 temperature. These findings suggest that local stratospheric cooling may be coupled to local
36 tropospheric warming.

37 1. Introduction

38 The Brewer-Dobson circulation (BDC) is a global-scale overturning circulation in the strato-
39 sphere, characterized by air that ascends into and within the tropical stratosphere, spreading
40 poleward and eventually downwards in the extratropical winter-hemisphere. This stratospheric
41 circulation can significantly impact tropospheric climate, most notably through its modulation of
42 the distribution of stratospheric ozone, which absorbs harmful ultraviolet radiation from the sun
43 (Dobson 1956). The widely accepted mechanism that explains the existence of the BDC is the
44 principle of “downward control” (Haynes and McIntyre 1987; Haynes et al. 1991). This principle
45 states that for steady circulations, the upward mass flux across a specified vertical level is solely a
46 function of the zonal momentum sources (wave-drag) and sinks above that level; thus, processes
47 in the middle and upper stratosphere can exert a “downward” influence on flow in the lower strato-
48 sphere and troposphere. The theoretical findings of Haynes et al. (1991) have been well supported
49 by numerical modeling evidence and withstood the test of time (Butchart 2014, and references
50 therein). Thus, in the “downward control” paradigm, wave dissipation drives the circulation.

51 The BDC is typically separated into two branches: a slow and deep equator-to-pole overturning
52 branch, and a faster shallow branch in the lower stratosphere extending to about 50° latitude (Plumb
53 2002; Birner and Bönisch 2011). In this study, references to the BDC refer to the shallow branch
54 circulation. The shallow branch is thought to be driven by sub-tropical wave-dissipation in the
55 lower stratosphere (Plumb and Eluszkiewicz 1999; Plumb 2002).

56 In our opinion, there are a few characteristics of the shallow branch circulation that remain
57 unresolved. First, calculations of residual vertical velocities at 70-hPa indicate off-equator maxima
58 in shallow branch upwelling in the summer-time hemisphere (Randel et al. 2008; Seviour et al.
59 2012). Even though wave-drag can force circulations non-linearly and non-locally, wave-drag
60 is at its annual maximum in the winter hemisphere, which is thus at odds with the observation
61 of tropical upwelling maximizing in the summer-time hemisphere (Holton et al. 1995; Plumb
62 and Eluszkiewicz 1999). In fact, all of the experiments performed in Plumb and Eluszkiewicz
63 (1999, hereafter, PE99) showed that as long as wave-drag maximizes in the winter hemisphere,
64 upwelling maximizes in the winter hemisphere. Only when thermal forcing was included, did
65 PE99 observe that upwelling maximizes in the summer hemisphere. Furthermore, at low latitudes,
66 a weak flow-dependent force (such as momentum diffusivity or linear damping) can be of leading
67 order importance in determining the steady circulation; as Plumb and Eluszkiewicz (1999) showed,
68 these weak forces, which can arise from thermal forcing, undermine the underlying hypothesis of
69 downward control, namely that the force can be specified independently of the applied heating. All
70 of this together implies that thermal forcing may be important in determining tropical stratospheric
71 upwelling.

72 In the tropical stratosphere, the observed upwelling strength is strongly correlated with tempera-
73 ture (Randel et al. 2006; Kerr-Munslow and Norton 2006), since a cold anomaly that slowly varies
74 in time must be maintained by adiabatic cooling against the effect of radiative heating. Therefore,
75 via downward-control arguments, wave-dissipation has been historically linked with tropopause
76 temperature. For instance, an annual cycle in sub-tropical wave-dissipation of equatorward prop-
77 agating extra-tropical waves has been suggested as responsible for the annual cycle in tropical
78 tropopause temperature (which is much larger in amplitude than that of the tropical troposphere)
79 (Yulaeva et al. 1994; Holton et al. 1995; Randel et al. 2002; Taguchi 2009; Garny et al. 2011; Kim
80 et al. 2016). Other studies have also attempted to understand how waves originating in the tropics
81 can explain various aspects of the tropopause region, including the annual cycle in temperature
82 (Boehm and Lee 2003; Norton 2006; Randel et al. 2008; Ryu and Lee 2010; Ortland and Alexander
83 2014; Jucker and Gerber 2017). In this view, the strength of zonally-symmetric upwelling in the
84 lower stratosphere is the primary control on zonally-symmetric temperature near the tropopause.

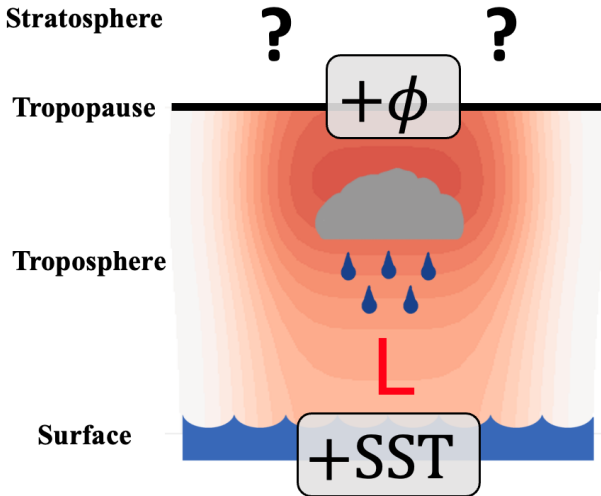
85 In contrast, many observational studies have found that, on a variety of space and time scales,
86 strong cold anomalies occur above regions of deep convection – in essence, local and regional
87 tropopause cooling is associated with local and regional tropospheric (Johnson and Kriete 1982;
88 Gettelman et al. 2002; Dima and Wallace 2007; Holloway and Neelin 2007; Kim and Son 2012;
89 Grise and Thompson 2013; Virts and Wallace 2014; Kim et al. 2018). There also seems to be
90 some spatial correlation between tropospheric warming and stratospheric cooling trends on global
91 warming time scales [see Fig. 1 of Fu et al. (2006)]. In general, the cold anomalies in the
92 lower stratosphere have been interpreted to be caused by convection itself, or forced from the
93 “bottom-up”. Since convection warms the troposphere, there is strong observational evidence of
94 an anti-correlation between tropospheric temperature and lower stratospheric temperature.

95 This oft-observed link between tropopause cooling and tropospheric warming has a number of
96 theoretical explanations. First, there is the hypothesis that convective overshooting (of the level of
97 neutral buoyancy) can cool the tropopause (Danielsen 1982; Sherwood 2000; Kuang and Bretherton
98 2004), emphasizing the role of convection in determining the mean temperature of the tropopause.
99 Holloway and Neelin (2007) offer an alternative hypothesis, and propose that a convective cold-top
100 forms via hydrostatic adjustment above tropospheric convective heating. This theory requires
101 that the associated pressure perturbation vanishes at some arbitrary level. Note that there is no
102 dependence of the temperature anomaly on the horizontal scale in this theory. Separately, some
103 authors have also argued that deep convection can excite a large-scale Kelvin wave response, which
104 also has a vertically tilted signature of tropopause cooling (Kiladis et al. 2001; Randel et al. 2003).
105 Finally, the anti-correlation in tropospheric temperature and lower stratospheric temperature has
106 also been explained through the vertical propagation of Rossby-waves (Dima and Wallace 2007;
107 Grise and Thompson 2013), though this theory is focused on sub-tropical regions, rather than on
108 the deep tropics. Regardless, most of these studies focus on daily to monthly time scales, and do
109 not consider how the observed lower stratospheric cold anomalies might affect lower stratospheric
110 upwelling more broadly. This is not trivial – while changes to the tropopause temperature that
111 project onto the zonal-mean could theoretically induce changes in shallow branch upwelling, a
112 corresponding, self-consistent change in the momentum budget must also occur to balance the
113 changes in the meridional circulation (Ming et al. 2016a).

If one persists with the assumption that the same mechanism responsible for local and regional scale anti-correlations between tropospheric warming and tropopause cooling can manifest itself at the zonally-symmetric scale (which is not a given), then it is perhaps unsurprising that there also exists a tight coupling between tropospheric warming and the BDC shallow branch mass flux, at least when using SST to characterize the tropical troposphere. In general circulation models (GCMs) and re-analyses, there are strong correlations between tropical-mean SST and the BDC shallow branch mass flux, across a wide variety of time scales (Lin et al. 2015; Orbe et al. 2020; Abalos et al. 2021). Fluctuations in tropical stratospheric upwelling have also been tied to ENSO (El Niño Southern Oscillation), one of the dominant sources of interannual tropical SST variability (Randel et al. 2009). In fact, interannual variations in tropical mean SST explain 40-50% of the interannual variability of the 70-hPa vertical mass flux (Lin et al. 2015; Abalos et al. 2021). In addition, nearly 70% of the CMIP6 model spread in the long-term trend of shallow branch mass flux is explained by the spread in tropical warming (Abalos et al. 2021).

The tight coupling between tropical SST and BDC shallow branch upwelling on interannual to climate change time scales has been explained through changes to the wave-drag, in light of the downward-control paradigm: surface warming leads to upper tropospheric warming and modification of the sub-tropical jets, which alters the upwards propagation and dissipation of mid-latitude waves in the sub-tropics (Garcia and Randel 2008; Calvo et al. 2010; Shepherd and McLandress 2011; Lin et al. 2015). While these theories can explain how SST and shallow branch mass flux are correlated, they were not constructed to also explain the oft-observed local-scale anti-correlation between SST and tropopause temperature.

In this study, we put forth an alternative explanation for the anti-correlation between tropospheric and lower stratospheric temperature. To start, consider the simplified atmospheric state shown in Figure 1, which has a troposphere in radiative convective equilibrium, with an overlying stratosphere at rest. Here, we assume that the tropopause acts as an infinitesimally small boundary between the troposphere and stratosphere, which neglects the existence of the tropical tropopause layer (TTL) (Fueglistaler et al. 2009), as further discussed in the conclusion. The TTL's role in the broader climate should not be neglected, especially since the TTL temperature has been linked with the concentration of water vapor in the stratosphere (Jensen and Pfister 2004; Fueglistaler et al. 2005; Randel et al. 2006; Randel and Park 2019).



149 FIG. 1. Schematic of a troposphere in radiative-convective-equilibrium, with an overlying stratosphere that
 150 is at rest. The troposphere is forced with a steady warm SST anomaly in the ocean. The troposphere warms
 151 (indicated by color shading) following a moist adiabat, the surface pressure falls, and the geopotential rises at
 152 the tropopause. How does the stratosphere respond to the an imposed tropopause geopotential anomaly?

144 This approximation notwithstanding, suppose we impose a steady patch of positive SST anomaly
 145 in the ocean. The increased surface enthalpy flux warms the troposphere, following a moist adiabat.
 146 The surface pressure falls, and the geopotential at the tropopause rises. Since there cannot be a
 147 pressure discontinuity across the tropopause, the pressure must also rise in the lower stratosphere.
 148 How far up does it extend, and what is the steady response in the stratosphere?

153 Section 2 tries to answer this conceptual question by introducing the concept of SST forcing
 154 of the tropopause and building a zonally asymmetric framework to understand the processes that
 155 control the upwards extent of tropopause anomalies. It is shown that there is a quasi-steady,
 156 quasi-balanced response of the stratosphere to tropospheric thermal forcing. Section 3 extends the
 157 analysis to the zonally-symmetric case, using a steady, coupled troposphere-stratosphere system
 158 to show how zonally symmetric SST anomalies (or, zonally symmetric tropospheric heating) can
 159 influence tropical upwelling in the lower stratosphere. Section 4 uses reanalysis data to argue for
 160 the real-world presence of the processes described in the proposed theory. Section 5 concludes the
 161 study with a summary and discussion.

162 **2. Stratospheric Response to a Tropopause Anomaly**

163 In this section, we introduce a simple conceptual model that will (1) illuminate how SST forcing
164 can induce a tropopause geopotential anomaly, and (2) understand what parameters modulate the
165 upwards extent of the tropopause anomaly into the stratosphere.

166 To understand how the stratosphere could be forced by the troposphere, we begin with tropo-
167 spheric dynamics. In radiative-convective equilibrium, a valid approximation is that of strict con-
168 vective quasi-equilibrium, where the saturation moist entropy, s^* , is constant with height (Emanuel
169 1987; Emanuel et al. 1994). Emanuel (1987) showed that linearized geopotential perturbations
170 are directly connected to linearized s^* perturbations (note here, for simplicity, we have ignored the
171 small effect of water vapor on density):

$$\frac{\partial \phi'}{\partial p} = - \left(\frac{\partial T}{\partial p} \right)_{s^*} s'^* \quad (1)$$

172 where prime superscripts indicate perturbation quantities. Since s^* is constant with height, Eq. 1
173 can be directly integrated in pressure to yield (as also shown in Lin and Emanuel (2022)):

$$\phi'(p) = \phi'_b + s'^* (\bar{T}_b - \bar{T}(p)) \quad (2)$$

174 where ϕ'_b is the perturbation boundary layer geopotential, \bar{T} is the basic state temperature, and \bar{T}_b
175 is the basic state boundary layer temperature. We non-dimensionalize according to:

$$\phi \rightarrow H^2 N^2 \phi \quad s^* \rightarrow \frac{H^2 N^2}{\bar{T}_b - [\bar{T}]} s^* \quad (3)$$

176 where H is the scale height, N^2 is the buoyancy frequency, and $[\bar{T}]$ is the basic state vertically-
177 averaged temperature. Dropping primes for perturbation quantities and non-dimensionalizing
178 yields:

$$\phi(p) = \phi_b + (1 - V_1(p)) s^* \quad (4)$$

179 where V_1 is the non-dimensional first baroclinic mode (Lin and Emanuel 2022):

$$V_1(p) = \frac{\bar{T}(p) - [\bar{T}]}{\bar{T}_b - [\bar{T}]} \quad (5)$$

180 Eq. 5 shows that the first baroclinic mode is positive near the surface, transitions to zero in the mid-
 181 troposphere, and is negative at the tropopause (which is evaluated at a fixed pressure). Evaluating
 182 Eq. 4 at the tropopause yields:

$$\phi(\hat{p}_t) = \phi_0 - V_1(\hat{p}_t)s^* \quad (6)$$

183 where \hat{p}_t is the non-dimensional tropopause pressure, and $\phi_0 = \phi_b + s^*$ is the barotropic geopotential.
 184 Note, the barotropic geopotential is constant with height. The total geopotential is the linear sum
 185 of the contributions of the tropospheric barotropic and baroclinic geopotential.

186 Since the tropopause is colder than the mean troposphere temperature, $V_1(\hat{p}_t)$ is negative, such
 187 that for positive SST anomalies ($s^{*''} > 0$), the tropopause geopotential anomaly will also be positive,
 188 provided the barotropic geopotential is not less than $V_1(\hat{p}_t)s^*$. In the real atmosphere, baroclinic
 189 perturbations are typically around an order of magnitude larger than barotropic ones (Lin and
 190 Emanuel 2022), such that for the sake of simplicity, we proceed with the approximation that ϕ_0 is
 191 small in relation to the baroclinic term. We will relax this assumption in the next section. Then, in
 192 this simple conceptual framework, we have a warm patch of ocean that imposes a steady positive
 193 geopotential anomaly at the tropopause.

194 Next, we will consider what happens to the stratosphere subject to a steady tropopause forcing
 195 (i.e. a steady lower boundary condition). The response of the stratosphere to external forcing has
 196 been well-studied using theoretical models [see Garcia (1987); Haynes et al. (1991); Plumb and
 197 Eluszkiewicz (1999), among many others]. However, the external forcing is typically presented in
 198 terms of being mechanical (wave-driven) or thermal in origin. We instead impose a tropopause
 199 forcing via the SST anomaly, and use the well-known quasi-geostrophic potential vorticity equations
 200 (QGPV), linearized about a resting basic state on an f-plane:

$$q'(x, y, z) = \frac{1}{f_0} \nabla_H^2 \phi' + \frac{f_0}{N^2} \frac{\partial^2 \phi'}{\partial z^2} - \frac{f_0}{HN^2} \frac{\partial \phi'}{\partial z} \quad (7)$$

201 where q is the potential vorticity (PV), f_0 is the Coriolis parameter, N is the buoyancy frequency,
 202 ϕ is the geopotential. Here, we are considering perturbations large enough in scale for the
 203 quasi-geostrophic approximation to apply. Dropping primes for perturbation quantities, assuming

204 wave-like solutions in the zonal and meridional [$\exp(ikx + ily)$], and non-dimensionalizing by:

$$\begin{aligned} x &\rightarrow Lx & y &\rightarrow Ly & z &\rightarrow Hz \\ \phi &\rightarrow H^2 N^2 \phi & q &\rightarrow f_0 q & t &\rightarrow t/f_0 \end{aligned} \quad (8)$$

205 where $L = NH/f$ is the Rossby radius of deformation, we obtain

$$\left(\frac{\partial^2}{\partial z^2} - \frac{\partial}{\partial z} - (k^2 + l^2) \right) \phi = q(z) \quad (9)$$

206 These equations can be found in most standard textbooks, e.g. section 5.4 of Vallis (2017). Here,
207 we emphasize the boundary conditions:

$$\phi(z=0) = \phi_T \quad (10)$$

$$\frac{\partial \phi}{\partial z}(z=\infty) = 0 \quad (11)$$

208 where the bottom boundary condition enforces continuity of pressure across the tropopause, given
209 the aforementioned tropopause geopotential anomaly that is imposed by an SST anomaly. The
210 upper boundary condition requires the temperature anomaly (or vertical velocity anomaly) be zero.
211 Though ϕ_T is imposed by the troposphere, via Eq. 6, in reality, barotropic motions are coupled to
212 the stratosphere. Thus, we can only assume the geopotential as a steady lower boundary condition,
213 and solve for the stratosphere in isolation, since we ignored the barotropic geopotential. As shall be
214 illuminated in the next section, the barotropic mode should really be coupled to the stratospheric
215 circulation.

216 We proceed by considering the stratospheric response to a geopotential anomaly at the tropopause,
217 with zero perturbation PV throughout the rest of the stratosphere. Since imposing a geopotential
218 anomaly at the tropopause has no direct effect on stratospheric PV, it can be considered as the fast
219 stratospheric response to a tropopause geopotential anomaly. In this textbook case, the solution is
220 straightforward:

$$\phi(z) = \exp(m_- z) \quad (12)$$

221 where

$$m_- = \frac{1 - \sqrt{1 + 4(k^2 + l^2)}}{2} \quad (13)$$

222 which shows that the geopotential anomaly decays in the vertical with a scale inversely proportional
223 to the horizontal scale of the anomaly. On re-dimensionalization, the Rossby penetration depth,

$$R_d = \frac{f_0 L}{N} \quad (14)$$

224 where L is the Rossby deformation radius, is the operative vertical scale of the geopotential.
225 Tropopause anomalies with large horizontal scales will extend deeper into the stratosphere than
226 smaller ones.

227 The temperature anomaly, scaling with $\frac{\partial \phi}{\partial z}$, will also decay exponentially with height according
228 to R_d . But how large can the temperature anomalies get? Thermal wind balance dictates that

$$g \frac{\partial \ln T}{\partial y} = -f \frac{\partial u}{\partial z} \quad (15)$$

229 If we take ∂z to scale as the Rossby penetration depth, then we obtain:

$$\ln T \approx \frac{Nu}{g} \quad (16)$$

230 Note that f drops out, which indicates that the temperature in the stratosphere does not directly
231 depend on f . It rather depends on the magnitude of the tropopause anomaly, as well as the
232 stratospheric stratification. For the case of zero perturbation PV in the stratosphere, the temperature
233 anomaly is just the geopotential anomaly multiplied by m_- , which is inversely proportional to the
234 horizontal scale of the tropopause PV anomaly. Therefore, the magnitude of the tropopause
235 temperature perturbations can be large for small horizontal scale anomalies, though these will
236 be confined to a rather shallow vertical layer near the equator (and may also not obey the quasi-
237 geostrophic approximation).

238 Next, it is instructive to consider how the stratosphere responds to the temperature anomalies.
239 As alluded to earlier, temperature anomalies disturb the radiative equilibrium of the stratosphere.
240 This must be associated with radiative heating anomalies. In this case, PV is no longer conserved.

241 The response of the stratosphere can be modeled as:

$$\frac{\partial q}{\partial t} = \frac{f_0}{N^2} \frac{\partial \dot{Q}}{\partial z} \quad (17)$$

242 where \dot{Q} is the heating rate (thermal forcing), and is parameterized to be a simple Newtonian
243 radiative relaxation:

$$\dot{Q} = -\alpha_r \frac{\partial \phi}{\partial z} \quad (18)$$

244 $\alpha_r > 0$ is the inverse time scale of the Newtonian radiative relaxation. Hitchcock et al. (2010) found
245 that linear radiative relaxation can explain around 80% of the variance in longwave heating rates
246 in a climate model, though this is less accurate in the lower stratosphere, and dependent on the
247 relaxation rate having a height-dependence. Non-dimensionalizing using Eq. 8, we obtain:

$$\frac{\partial q}{\partial t} = -\gamma \frac{\partial^2 \phi}{\partial z^2} \quad (19)$$

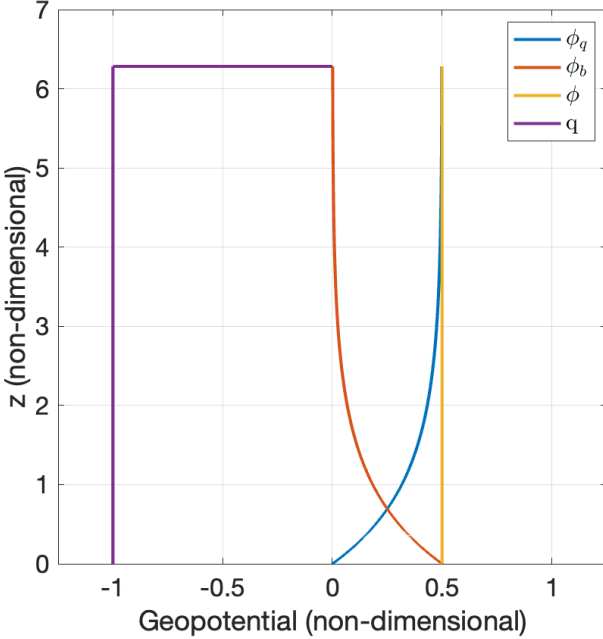
248 where $\gamma = \alpha_{\text{rad}}/f_0$.

249 The effect of radiative damping on stratospheric circulations has been thoroughly explored in a
250 number of early theoretical studies (Garcia 1987; Haynes et al. 1991; Haynes and Ward 1993). In
251 particular, the seminal work of Haynes et al. (1991) showed that in zonally symmetric, radiatively
252 damped, time-dependent systems whereby a steady mechanical forcing is instantaneously applied,
253 there is an adjustment to a barotropic state (in u) above the level of forcing. Our set up is similar to
254 the model outlined in section 3 of Haynes et al. (1991), except here the steady forcing is restricted
255 to the tropopause geopotential – the forcing is neither wave-driven nor thermal in origin.

259 To solve for the geopotential, the Green's function (see the Appendix) is convoluted with the
260 source term under the lower boundary condition:

$$q_T = -k_m \phi_T \quad (20)$$

261 where $k_m = k^2 + l^2$ is the total wavenumber. This can be calculated numerically (see the Appendix
262 for more details). Figure 2 shows the stratospheric geopotential solutions that describe the initial and
263 final states after imposing a tropopause geopotential anomaly. The initial geopotential distribution
264 from the steady geopotential anomaly is shown as ϕ_b , and is just the zero interior perturbation



256 FIG. 2. The geopotential associated with (red) a boundary PV anomaly of $q = -1$ (ϕ_b), (blue) a constant PV
 257 anomaly of $q = -1$ in the interior (ϕ_q), and (yellow) the sum of the two ($\phi = \phi_q + \phi_b$). The corresponding total
 258 PV is shown in purple. Here we assume $k_m = 2$, and $z_{\text{top}} = 1 + 2\pi$.

265 PV solution mentioned earlier in the text, where the response decays exponentially with height.
 266 The geopotential distribution associated with the generation of anomalous PV through diabatic
 267 heating by radiative relaxation is shown in ϕ_q , while the total geopotential is shown as $\phi = \phi_q + \phi_b$.
 268 The total geopotential is constant with height (barotropic) above the level of forcing, as found by
 269 Haynes et al. (1991).

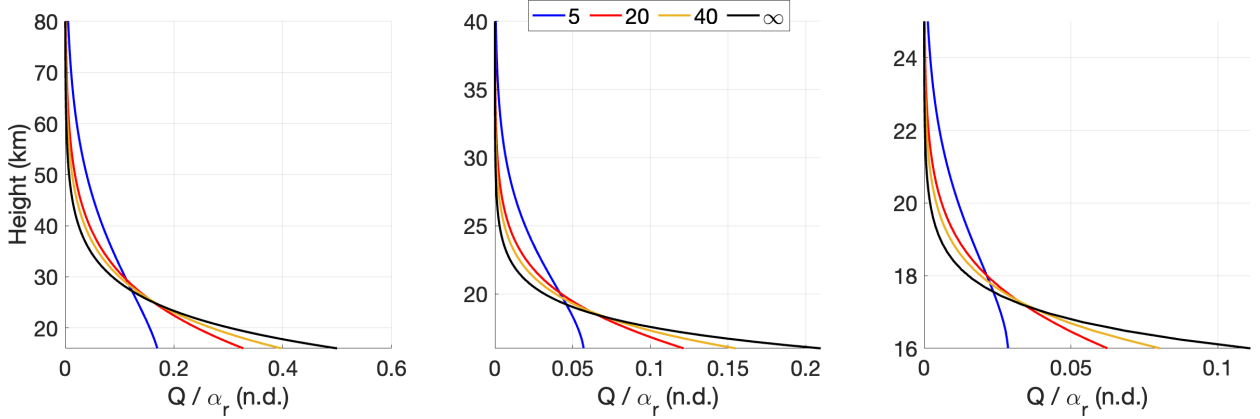
270 A simple physical picture is painted with this conceptual model that can provide an rather
 271 straightforward answer to the schematic shown in Figure 1. If the troposphere is forced with a
 272 steady positive SST anomaly, a positive geopotential anomaly forms at the tropopause. A positive
 273 tropopause geopotential anomaly is initially accompanied with a cold anomaly in the stratosphere,
 274 which is associated with radiative heating and rising motion. If this process is allowed to proceed
 275 towards a steady state back to radiative equilibrium, the geopotential and PV must eventually
 276 become constant with height (i.e. barotropic), as implied by Eq. 18, and the temperature anomaly
 277 in the stratosphere disappears. In this way, the troposphere can force the stratosphere, at least on
 278 the steady time scales considered here. This also shows that the geopotential does not have to go

279 to zero at the upper boundary. The only requirement is that the energy density goes to zero. Thus,
280 the assumption of the geopotential going to zero at the upper boundary in Holloway and Neelin
281 (2007) seems arbitrary.

282 How long does it take to reach the barotropic state? Haynes et al. (1991) showed that in the
283 zonally symmetric case, the adjustment towards a barotropic state above the level of forcing occurs
284 with an upward propagation speed of $w_\alpha = \alpha_{\text{rad}} R_d^2 / H_s$. In the tropics, w_α is small, owing to the
285 smallness of both α_{rad} and R_d . For an anomaly of horizontal scale around 5000 km at a latitude of
286 10°, and a radiative relaxation time scale of $\alpha_{\text{rad}} = 20 \text{ days}^{-1}$, $w_\alpha \approx O(10^{-1}) \text{ mm s}^{-1}$ – an upward
287 propagation of only a few km per year. It is also possible to numerically calculate the amount of
288 time it takes for the system to reach its final barotropic state, by time-stepping Eq. 19 forwards in
289 time while holding the lower-boundary PV fixed. For a stratosphere with a depth of around 32-km
290 ($z_{\text{top}} = 4$ for a scale height of $H_s = 8 \text{ km}$), assuming $\gamma = 0.02$ and a Coriolis parameter akin to that
291 at 10° latitude, it takes around 3 years for the system to become barotropic.

292 This long relaxation time makes it unlikely that the barotropic state is ever reached in the real
293 stratosphere, since unsteady processes can disrupt the simple state assumed in this model. For
294 instance, tropospheric thermal forcing does not remain steady on the order of years, as there is a
295 seasonal cycle in heating. Furthermore, since the β -effect is not included in this simple framework,
296 we also ignore the possibility of the excitation of large-scale waves (and their corresponding effects)
297 as a part of the response to tropospheric thermal forcing.

298 Indeed, the vertical propagation of planetary waves into the stratosphere has been cited as one
299 potential reason for the observed anti-correlation between tropospheric and lower stratospheric
300 temperature (Dima and Wallace 2007; Grise and Thompson 2013). Here, we offer an alternative
301 perspective, by returning to the schematic shown in Figure 1. In the case that there is constant
302 Coriolis force everywhere, there would be no stationary Rossby wave associated with tropospheric
303 heating. But, at least according to the proposed theory, a cold anomaly (that is not related to
304 convective overshooting) would still form above the tropopause. Of course, in the real world, β
305 allows for a steady wave response (Gill 1980) that could disrupt the simple atmospheric state we
306 have proposed. In this case, the quasi-balanced response of the stratosphere could occur in tandem
307 with the vertical propagation of planetary waves [which are excited as part of the tropospheric
308 thermal forcing], though a thorough investigation of this is left to future work.



309 FIG. 3. (Left) The diabatic heating profile (Q/α_r) with height in the stratosphere after 30 days of integration,
 310 subject to a steady tropopause boundary forcing with a horizontal scale of around 28000-km, and a (blue) 5-day,
 311 (red) 20-day, (yellow) 40-day. The vertical derivative of the geopotential for the zero-PV stratospheric response
 312 to a tropopause forcing (infinite radiative relaxation time scale) is shown in black. (Middle) and (Right) are the
 313 same as top but for a horizontal scale of around 9500-km, and 4500-km, respectively. We assume a latitude of
 314 10°, a scale height of 8 km, and a tropopause height of 16 km to convert to dimensional height. Note the vertical
 315 scale varies in each subplot, for detail.

316 In light of this, the intermediate states between the fast stratospheric response [ϕ_b in Figure 2]
 317 in which the anomaly decays exponentially with height, and the barotropic steady-state response
 318 in which the boundary anomaly is communicated throughout the depth of the stratosphere [ϕ in
 319 Figure 2], could be important. For practical purposes, the geopotential anomaly is not as important
 320 as the associated radiative heating, which is potentially important for tracer transport into the
 321 stratosphere. Figure 3 shows the non-dimensional diabatic heating profiles with height after 30
 322 days of integration, for a stratosphere subject to an imposed tropopause geopotential anomaly
 323 that is associated with a unitary non-dimensional anticyclonic PV, under varying magnitudes of
 324 stratospheric radiative relaxation rates. The diabatic heating profiles are normalized by the radiative
 325 relaxation rate. For comparison purposes, we show the temperature anomaly associated with the
 326 (time-independent) zero perturbation PV geopotential solution (i.e. an infinite radiative-relaxation
 327 time scale), even though there is no associated diabatic heating, by definition. Figure 3 shows
 328 that after 30-days, there is non-trivial lifting (in height) of the diabatic heating anomaly over

329 time. The stronger the strength of radiative relaxation, the faster the diabatic heating anomaly is
330 communicated into the stratosphere.

331 These calculations show that tropospheric heating imposes a positive tropopause geopotential
332 anomaly, which elicits a quasi-balanced response in the stratosphere. The fast stratospheric response
333 is simply an anomaly that decays in the vertical according to the Rossby penetration depth. On
334 slower time scales, radiative relaxation induces an upward migration of the anomaly. The radiative
335 relaxation rate, the horizontal scale of the anomaly, and the Coriolis parameter all determine the
336 upward migration rate, as shown in Haynes et al. (1991). Thus, the ensuing, time-dependent
337 temperature response in the stratosphere is also tied to these parameters. In the next section, we
338 will elaborate on the ideas put forth in this conceptual model in a zonally-symmetric framework,
339 and analyze, in detail, the sensitivity of the stratospheric response to tropospheric forcing, with
340 regards to these parameters.

341 **3. Troposphere-Stratosphere Response to SST**

342 In the previous section, we used a simple QGPV framework to understand how a SST anomaly
343 can impose a tropopause geopotential anomaly and therefore elicit a quasi-balanced response in the
344 stratosphere. However, we used the tropopause as a lower boundary condition for the stratosphere
345 when in reality, the tropopause and stratosphere are coupled. In this section, we develop a simple,
346 zonally-symmetric, coupled troposphere-stratosphere model, and explore how radiation and wave-
347 drag can modulate the response of the stratosphere to SST forcing.

348 *a. Model Formulation*

349 Lin and Emanuel (2022) formulated a linear, coupled troposphere-stratosphere model, but in
350 the context of unsteady equatorial waves. In that linear system, a convecting, quasi-equilibrium
351 troposphere was coupled to a dry and passive stratosphere. We use the same non-dimensional
352 system derived in Lin and Emanuel (2022), except we only consider steady, zonally symmetric

353 circulations. The tropospheric system is governed by:

$$yv_0 - F(u_0 + u_1) = 0 \quad (21)$$

$$-\frac{\partial \phi_0}{\partial y} - yu_0 = 0 \quad (22)$$

$$yv_1 - F(u_0 + u_1) - D_t u_1 = 0 \quad (23)$$

$$yu_1 = \frac{ds^*}{dy} \quad (24)$$

$$\frac{\partial v_0}{\partial y} + \frac{\partial v_1}{\partial y} + \frac{\partial \omega}{\partial y} = 0 \quad (25)$$

354 where u_0 and v_0 are the barotropic zonal and meridional winds (constant with height), u_1 and v_1
 355 are the baroclinic zonal and meridional winds, ϕ_0 is the barotropic geopotential, s^* is the saturation
 356 moist entropy (that is assumed to be vertically constant, as in a quasi-equilibrium troposphere), D_t
 357 is a non-dimensional Rayleigh damping coefficient, and

$$F = \frac{aC_d|\bar{\mathbf{V}}|}{\beta L_y^2 h_b} \quad (26)$$

358 is a non-dimensional surface friction coefficient (derived in Lin and Emanuel (2022)), where C_d
 359 is the drag coefficient, h_b is the boundary layer depth, L_y is the meridional length scale, β is the
 360 meridional gradient of the Coriolis force, a is the radius of the Earth, and $\bar{\mathbf{V}}$ is the basic state
 361 surface wind speed magnitude. The vertical structure of the baroclinic variables are determined
 362 by V_1 (Eq. 5). Note that while there are equations for the tropospheric thermodynamics in Lin and
 363 Emanuel (2022), they are omitted here. Since s^* is taken to be specified, representative of a SST
 364 forcing, there are 6 unknown variables, $(u_0, u_1, v_0, v_1, \omega, \phi_0)$ and 5 equations. The system will be
 365 completed with a formulation of boundary conditions that will couple the troposphere system to a
 366 stratosphere (and provide the last equation).

367 In the ensuing text, terms with an overlying hat are dimensional. \hat{D}_t , the (dimensional) inverse
 368 time scale of the Rayleigh damping coefficient is:

$$\hat{D}_t \rightarrow \frac{\beta L_y^2}{a} D_t \quad (27)$$

369 In Eq. 23, $D_t u_1$ acts as a relaxational wave drag on the zonal flow. It does not act on the coupling
 370 between the troposphere and stratosphere, and is only used to diagnose v_1 (which by definition,
 371 has a value of zero at the tropopause). Thus, D_t modulates the baroclinic vertical velocity profile
 372 in the zonally symmetric meridional overturning circulation.

373 As formulated, the tropospheric system represents an atmosphere in which temperature anomalies
 374 in the vertical are restricted to follow the moist adiabat. The associated baroclinic mode, which is
 375 forced through surface enthalpy fluxes (s^*), can then excite the barotropic mode through surface
 376 friction (Lin and Emanuel 2022). The barotropic mode then excites the stratosphere. However,
 377 the stratospheric circulation becomes uncoupled with the tropospheric circulation when $F = 0$ – in
 378 this case, the tropospheric solution simply obeys Eqs. 23-25, and the barotropic mode (as well as
 379 the stratospheric state to tropospheric forcing) becomes ill-defined. This implies that friction has
 380 an outsized influence on stratospheric circulations. However, this may not be true in reality, since
 381 the barotropic mode can also be coupled to the baroclinic mode through non-linearity and vertical
 382 wind shear. Both of these processes are not represented in this work.

383 The stratosphere is formulated in log-pressure coordinates and assumed to be in hydrostatic
 384 balance [see Chapter 3 of Andrews et al. (1987)]. The steady, linear, zonally symmetric, non-
 385 dimensional equations of the stratosphere are also derived from the system used in Lin and
 386 Emanuel (2022), and summarized below:

$$yv_s - D_s u_s = 0 \quad (28)$$

$$-\frac{\partial \phi_s}{\partial y} - yu_s = 0 \quad (29)$$

$$\frac{\partial v_s}{\partial y} + \frac{1}{\rho_s} \frac{\partial(\rho_s w_s)}{\partial z^*} = 0 \quad (30)$$

$$w_s S = -\alpha_{\text{rad}} \frac{\partial \phi_s}{\partial z} \quad (31)$$

$$\rho_s = \exp\left(\frac{H}{H_{s,s}}(1 - z^*)\right) \quad (32)$$

387 where subscripts denote quantities in the stratosphere, w_s is the log-pressure vertical velocity, S is
 388 a non-dimensional stratospheric stratification, ρ_s is the basic state density, H is the dimensional
 389 tropopause height, $H_{s,s}$ is the dimensional scale height in the stratosphere, the log-pressure ver-
 390 tical coordinate $z^* \equiv -H \ln(p/p_t) + 1$ is defined such that $z^* = 1$ is the bottom boundary, or the

391 tropopause, and α_{rad} is the non-dimensional radiative damping time scale in the stratosphere:

$$\hat{\alpha}_{\text{rad}} \rightarrow \frac{\beta L_y^2}{a} \alpha_{\text{rad}} \quad (33)$$

392 Relaxational wave drag, $D_s u_s$, is included only in the zonal momentum equations, as similarly used
393 by Plumb and Eluszkiewicz (1999). It is not necessary that $D_s = D_t$, though discontinuities in the
394 meridional velocity at the tropopause will occur if $D_s \neq D_t$. This form of wave drag is simplistic,
395 and it is a rather poor representation of the response of the circulation to external forces (Ming
396 et al. 2016b).

397 Finally, S plays an important role in the behavior of this model, and is:

$$S = \frac{N^2 H^2}{\beta^2 L_y^4} \quad (34)$$

398 where N is the buoyancy frequency. Note, there is no explicitly imposed thermal or mechanical
399 forcing in the stratosphere. Thus, we consider a stratosphere entirely forced from the troposphere.

400 *b. Stratospheric response to tropopause forcing*

401 In the case of an isolated stratosphere subject to a tropopause forcing, the stratospheric equations
402 can be reduced to a single differential equation for the geopotential:

$$\frac{\partial^2 \phi}{\partial z^2} - \frac{H}{H_{s,s}} \frac{\partial \phi}{\partial z} + \frac{\xi}{y^2} \left[\frac{\partial^2 \phi}{\partial y^2} - \frac{2}{y} \frac{\partial \phi}{\partial y} \right] = 0 \quad (35)$$

403 where

$$\xi = \frac{D_s S}{\alpha_{\text{rad}}} = \frac{\hat{D}_s}{\hat{\alpha}_{\text{rad}}} \frac{N^2 H^2}{\beta^2 L_y^4} \quad (36)$$

404 is a non-dimensional term that depends on the ratio between the time scale of wave-drag to that
405 of radiation. This quantity is equivalent to a "dynamical aspect ratio" that describes the ratio of
406 the vertical to horizontal scale of the circulation response to an imposed forcing (Garcia 1987;
407 Plumb and Eluszkiewicz 1999; Haynes 2005; Ming et al. 2016b). As detailed in Ming et al.
408 (2016b), who incorporated an additional external heating in the stratosphere, when the aspect
409 ratio is large ($\xi \gg 1$), the external heating is narrow and primarily balanced by upwelling, and

410 when the aspect ratio is small ($\xi \ll 1$), the external heating is broad and primarily balanced by
 411 Newtonian cooling. In this study, the interpretation of ξ does not have exactly the same meaning,
 412 since we do not impose a temperature-independent external heating to the system (which in the
 413 real world would arise from absorption of radiation by ozone) – our simple system is instead forced
 414 via the tropopause geopotential, and upwelling always balances Newtonian cooling. Here, ξ better
 415 describes the geopotential response with height. As we shall see later, when the radiative time scale
 416 is much faster than the wave-drag time scale ($\xi \ll 1$), the meridional derivative terms are small and
 417 the system will become nearly barotropic in the vertical. On the other hand, when the wave-drag
 418 time scale is much faster than the radiative time scale ($\xi \gg 1$), the stratospheric signature of the
 419 tropopause anomaly is muted. Note the presence of L_y , which indicates the importance of the
 420 horizontal scale of the anomaly.

421 Eq. 35 can be solved numerically, discretizing the grid in the meridional and vertical directions.
 422 The stratospheric geopotential is also subject to a zero temperature anomaly at the top of the
 423 domain, or equivalently, zero derivative of the geopotential. The geopotential anomaly is enforced
 424 to be zero on the northern and southern borders. For illustrative purposes, we first solve the
 425 equations under a fixed lower boundary condition:

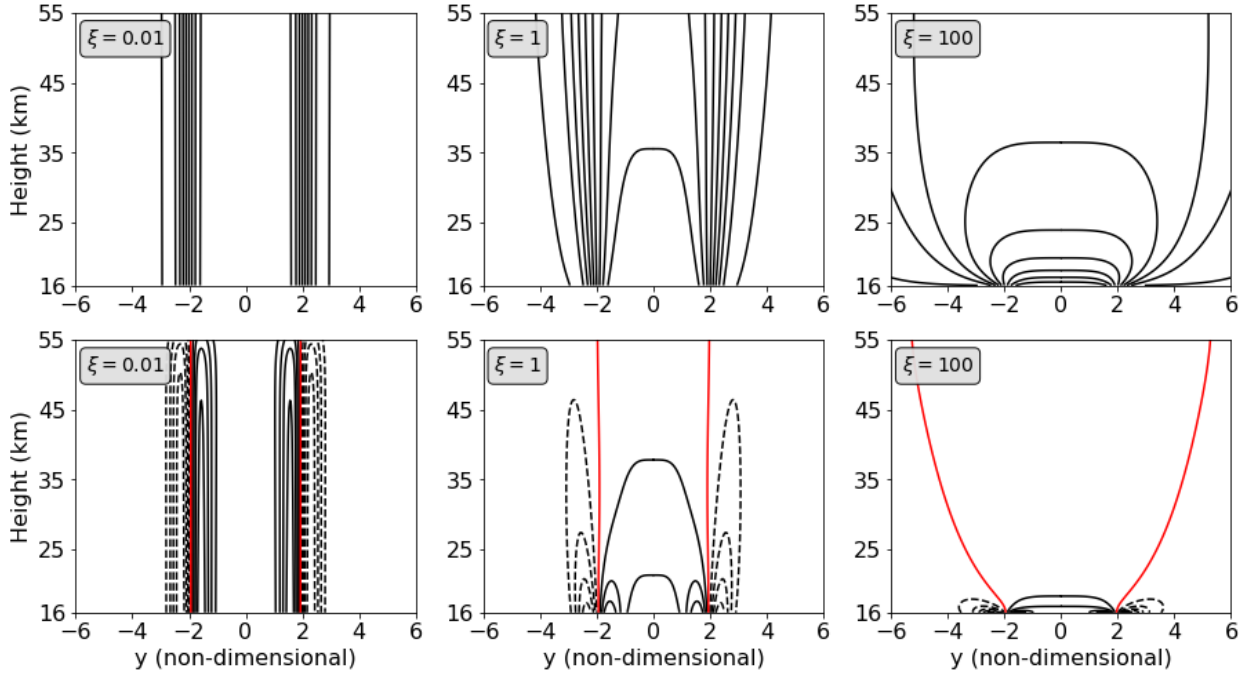
$$\phi(z^* = 1) = \phi_T \quad (37)$$

426 where

$$\phi_T = \int_y y \exp(-4(y-2)^2) - y \exp(-4(y+2)^2) \quad (38)$$

427 This represents a flat positive geopotential anomaly in the tropics (tropical heating) that decays to
 428 zero in the subtropics. As will become clear later when the solutions are coupled to the troposphere,
 429 this geopotential structure is associated with sub-tropical jets at $y = \pm 2$.

430 Figure 4 shows the stratospheric response to a tropopause geopotential anomaly, under varying
 431 values of ξ . Here, the numerical calculations confirm the mathematical analysis. Indeed, for
 432 $\xi = 0.01$ (i.e. when wave-drag is very weak), radiation acts to create a nearly barotropic stratosphere,
 433 in which motion is confined to constant angular momentum surfaces. The vertical structure of the
 434 vertical velocity in this case is qualitatively similar to the thermally forced vertical mode calculated
 435 in PE99 [see their Fig. 11]. When the time scale of wave-drag is faster than radiation ($\xi = 100$),



430 FIG. 4. (Top-row) The zonally symmetric geopotential response to an imposed tropopause geopotential
 431 anomaly, as shown in Eq. 38, for varying values of ξ . (Bottom-row) Same as the top-row except for the zonally
 432 symmetric vertical velocity response. The red-line is the zero vertical velocity isoline. Tropopause height is
 433 16-km, and stratospheric scale height is 8-km.

440 the vertical penetration of the tropopause geopotential anomaly is significantly muted. In fact, the
 441 vertical velocity anomalies only extend on the order of a few km into the stratosphere. In this
 442 sense, the relaxational wave-drag acts to both mute the vertical scale of the tropopause geopotential
 443 anomaly, and sustain a meridional overturning circulation.

444 As elaborated on earlier, there is much existing theoretical work that shows the response of
 445 the stratosphere to an external forcing is dependent on the strength of wave-drag, the strength
 446 of radiative relaxation, and the aspect ratio of the tropopause anomaly (Garcia 1987; Haynes
 447 et al. 1991; Ming et al. 2016b). This work is mathematically similar to and agrees with the
 448 aforementioned studies. Unlike the others, this work emphasizes the role of tropopause forcing on
 449 the stratosphere, and introduces the idea that there is a quasi-balanced response in the stratosphere
 450 to tropopause forcing, via tropospheric heating.

451 *c. Tropospheric forcing of stratospheric upwelling*

452 Next, we couple the stratospheric equations to the zonally symmetric tropospheric equations, to
 453 show how tropospheric thermal forcing can influence stratospheric upwelling. In order to couple
 454 the troposphere and stratosphere, we use classical matching conditions: (1) continuity of pressure
 455 (geopotential) and (2) vertical velocity at the tropopause:

$$\phi_s(z^* = 1) = \phi_T \quad (39)$$

$$B\omega(\hat{p}_T) = -w_s(z^* = 1) \quad (40)$$

456 where $B = \frac{H_{s,t}}{H} \frac{p_s - p_t}{p_t}$ is a scaling coefficient between pressure velocity and vertical velocity (Lin
 457 and Emanuel 2022). Here, p_s is the surface pressure, p_t is the tropopause pressure, and $H_{s,t}$ is the
 458 scale height of the troposphere. Solving for v_0 using Eqs. 25, 39, 40, and assuming zero flow at
 459 the boundaries, yields:

$$v_0 = \frac{\alpha_{\text{rad}}}{SB} \int_y \left. \frac{\partial \phi_s}{\partial z} \right|_{z^*=1} dy \quad (41)$$

460 Here we see that under a rigid lid condition, where $S \rightarrow \infty$, $v_0 = 0$. In addition, B is proportional
 461 to the troposphere scale height, which itself is inversely proportional to the dry stratification of
 462 the troposphere. Hence, SB can also be thought of as a scaled ratio of the troposphere buoyancy
 463 frequency to the stratosphere buoyancy frequency. The strength of radiative relaxation also appears
 464 in the numerator. This is because the magnitude of the tropospheric barotropic mode is determined,
 465 in part, by stratospheric dynamics.

466 Eqs. 21 and 24 are used to solve for u_0 in terms of the stratosphere and the external forcing:

$$u_0 = y \frac{1}{\xi \gamma} \int_y \left. \frac{\partial \phi_s}{\partial z^*} \right|_{z^*=1} dy - \frac{1}{y} \frac{ds^*}{dy} \quad (42)$$

467 where

$$\gamma = \frac{FB}{D_s} \quad (43)$$

468 is an additional non-dimensional parameter that qualitatively represents the ratio between strato-
 469 spheric and tropospheric drag (there is tropospheric wave drag, but it does not act on the barotropic
 470 mode, only on the baroclinic mode). γ is not entirely independent from ξ , since D_s appears in both.

471 Again, under the rigid lid condition, $\xi \rightarrow \infty$, such that the barotropic zonal wind becomes only a
 472 function of the tropospheric forcing. Note again that when $F = 0$, the barotropic mode becomes
 473 ill-defined, since it is no longer coupled to the baroclinic mode.

474 In order for the continuity of pressure to be satisfied, the geopotential at the lower boundary of
 475 the stratosphere must satisfy Eqs. 6 and 39. Combining Eqs. 6, 22, 39, and 42 yields:

$$\frac{\partial \phi_s}{\partial y} \Big|_{z^*=1} - y^2 \frac{1}{\xi \gamma} \int_y \left(\frac{\partial \phi_s}{\partial z} \right) \Big|_{z^*=1} dy = (1 - V_1(\hat{p}_t)) \frac{ds^*}{dy} \quad (44)$$

476 which is an equation for the boundary geopotential entirely in terms of the external forcing, s^* .
 477 The Rayleigh damping coefficient for stratospheric wave-drag does not appear in the boundary
 478 condition, since

$$\frac{1}{\xi \gamma} = \frac{\alpha_{\text{rad}}}{D_s S} \frac{D_s}{FB} = \frac{\alpha_{\text{rad}}}{SFB} \quad (45)$$

479 When $\xi \gamma$ is large, the boundary condition simply reduces to Eq. 6, with $\phi_b = 0$. When $\xi \gamma$ is
 480 small, s^* becomes a multiple of a double integral in y of the vertical derivative of the stratospheric
 481 geopotential at the tropopause.

482 Incorporating Eq. 44 as the lower boundary condition is numerically tricky given the meridional
 483 integral, since it precludes the inversion of a sparse matrix. The integral can be removed by dividing
 484 by y^2 and differentiating with respect to y , which yields:

$$\frac{-2}{y^3} \frac{\partial \phi_s}{\partial y} + \frac{1}{y^2} \frac{\partial^2 \phi_s}{\partial y^2} - \frac{1}{\xi \gamma} \frac{\partial \phi_s}{\partial z} = (1 - V_1(\hat{p}_t)) \left(\frac{1}{y^2} \frac{d^2 s^*}{dy^2} - \frac{2}{y^3} \frac{ds^*}{dy} \right) \quad (46)$$

485 where the entire equation is evaluated at $z^* = 1$. This boundary condition leads to a sparse matrix
 486 that can be easily incorporated into a numerical solver.

487 Before continuing with the numerical solutions, we formulate the SST forcing in the troposphere.
 488 We observe from Eq. 24 that:

$$s^* = \int y u_1 dy \quad (47)$$

489 such that we can specify the baroclinic wind response to obtain a suitable s^* anomaly. Here, we
 490 specify:

$$u_1(y) = -\exp(-4(y-2)^2) - \exp(-4(y+2)^2) \quad (48)$$

491 which is akin to subtropical jets symmetric about the equator. Note, the meridional baroclinic wind
 492 is:

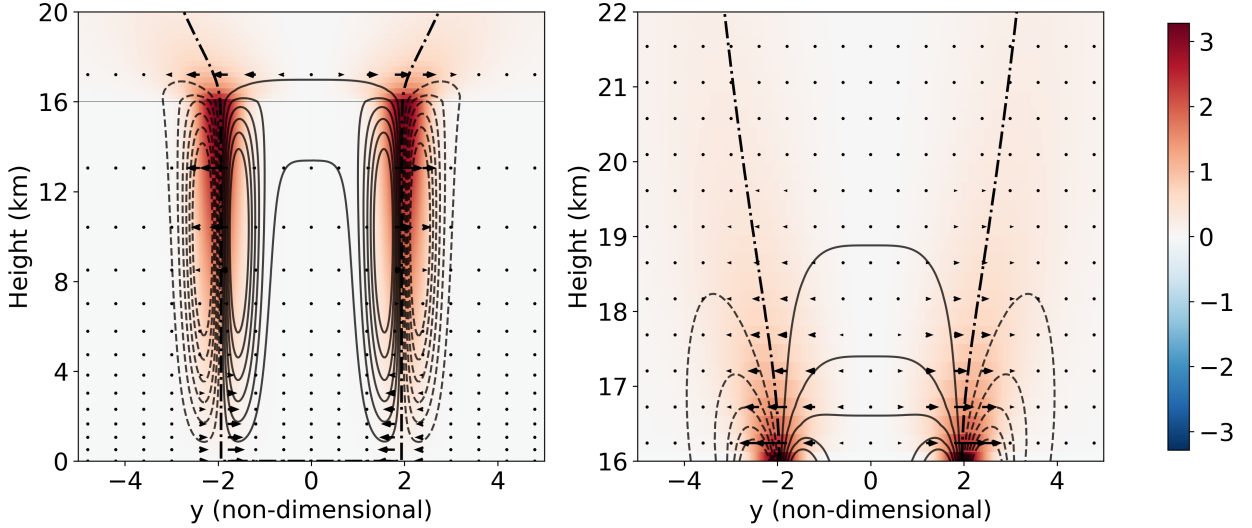
$$v_1 = \frac{F}{y} u_0 + \frac{D_t + F}{y^2} \frac{ds^*}{dy} \quad (49)$$

493 Numerical evaluation of v_1 requires that the meridional derivative of s^* go to zero faster than y^2
 494 in the limit of $y \rightarrow 0$, otherwise v_1 will become unstable for small values of y on the numerical
 495 grid. However, the stratospheric solution does not depend on v_1 , so this constraint merely ensures
 496 a smoothly varying tropospheric circulation. Thus, $u_1(y)$ is chosen to satisfy this constraint. We
 497 proceed by numerically solving the stratospheric system (Eq. 35) with the modified boundary
 498 condition shown in Eq. 46, as well as the s^* forcing shown in Eq. 47. See the appendix for more
 499 details on the numerical solver.

500 To set the non-dimensional parameters of the model, we use Earth-like parameters of
 501 $N^2 = 6 \times 10^{-4} \text{ s}^{-2}$, $H = 16 \text{ km}$, $H_{s,t} = H_{s,s} = 8 \text{ km}$, $\beta = 2.3 \times 10^{-11} \text{ s}^{-1} \text{ m}^{-1}$, $L_y = 1200$
 502 km (such that $y = 1$ represents approximately ten degrees of latitude), $C_d = 10^{-3}$, $|\mathbf{V}| = 3 \text{ m s}^{-1}$.
 503 Furthermore, we choose $T_b = 303 \text{ K}$, a surface pressure of 1000-hPa, and a tropopause pressure of
 504 100-hPa. The vertical temperature profile in the troposphere follows a pseudoadiabatic lapse rate
 505 (neglecting changes to heat capacity, see Eq. 4.7.5 of Emanuel (1994)), such that $[\bar{T}] \approx 264.5 \text{ K}$
 506 and $\bar{T}(p_t) \approx 176.1 \text{ K}$. With these values, $V_1(p_t) \approx -2.3$.

507 Since α_{rad} and \hat{D}_t play critical roles in the stratospheric response to an imposed tropopause
 508 geopotential anomaly, we will explore the the non-dimensional space of ξ and γ . Still, it is helpful
 509 to note the estimates of the general order of magnitudes of these quantities in the real stratosphere.
 510 Hitchcock et al. (2010) estimated the radiative relaxation time scale to be approximately 25 days in
 511 the lower tropical stratosphere. The magnitude of the Eliassen Palm (EP) flux divergence is around
 512 $O(1) \text{ m s}^{-1} \text{ day}^{-1}$ in the subtropics, but decays rapidly as one moves equatorward into the deep
 513 tropics (Randel et al. 2008). For a perturbation zonal wind speed of $O(10) \text{ m/s}$, this corresponds
 514 to a Rayleigh damping rate of around 10 days^{-1} and slower.

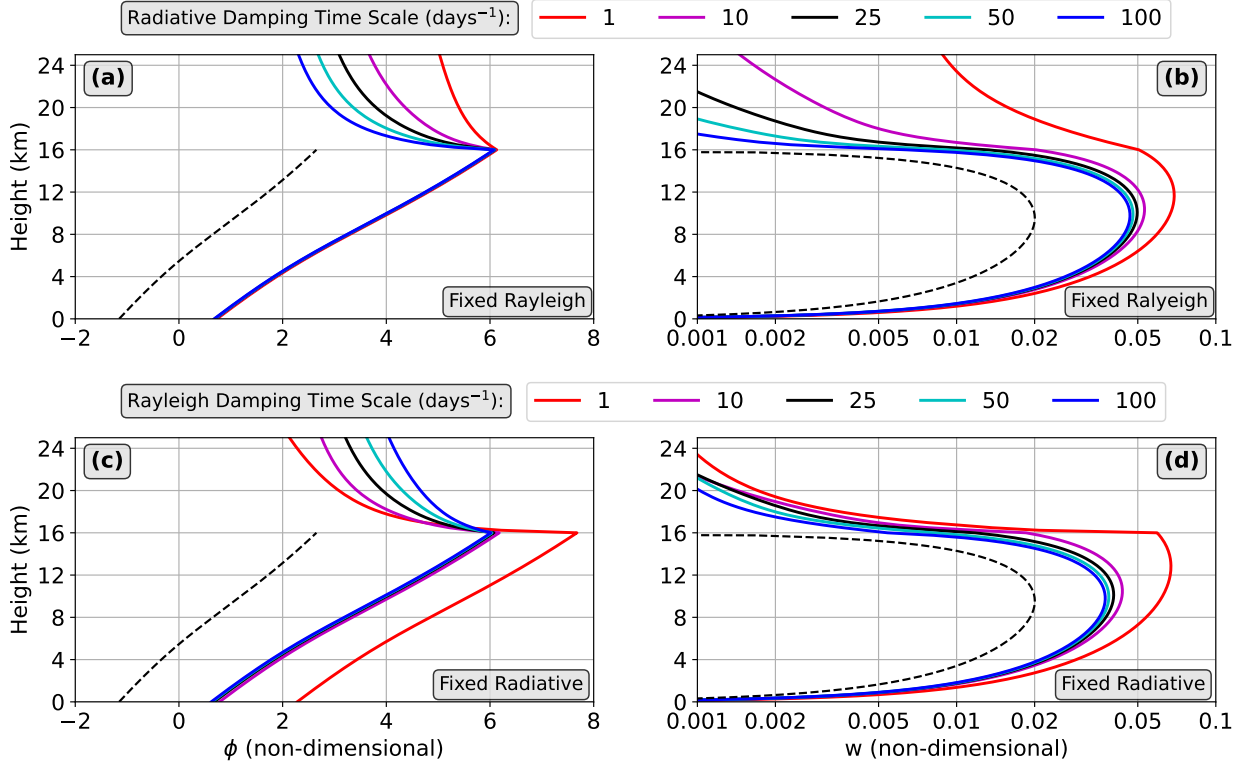
520 For now, we restrict the analysis to "Earth-like" parameters, with $\hat{\alpha}_{\text{rad}} = 25 \text{ days}^{-1}$, and
 521 $\hat{D}_s = \hat{D}_t = 25 \text{ days}^{-1}$. This choice leads to $\xi \approx 150$ and $\gamma \approx 30$. Thus, $\xi\gamma$ is large, and
 522 the tropopause geopotential can be approximated as simply a multiple of s^* . Figure 5 shows the
 523 zonally symmetric, linear response to the prescribed, equatorially symmetric SST forcing. We
 524 observe a meridionally shallow, thermally direct overturning circulation in the troposphere, associ-



515 FIG. 5. (Left): The zonally symmetric response to a SST (s^*) forcing shown in Eq. (47). Zonal winds are
 516 shown in colors (red for westerlies), contours show vertical motion (w), with contour spacing of 0.005, starting
 517 at 0.03. Dot-dashed line is the zero w iso-line, and arrows show the meridional motion. The tropopause is shown
 518 by the thin gray line. “Earth-like” parameters of $\xi = 150$, $\gamma = 30$ are used. (Right): Same as left, but zoomed in
 519 on the stratosphere. Contour spacing is 0.002, starting at 0.01.

525 ated with sub-tropical jets at $|y| = 2$ that decay exponentially with height into the stratosphere. The
 526 tropopause geopotential is elevated in the tropical region ($|y| < 2$) (not shown). Associated with
 527 this elevated tropopause geopotential is a weak, meridionally shallow, thermally indirect overturning
 528 circulation in the stratosphere, with upwelling around an order of magnitude smaller than peak
 529 upwelling in the troposphere. Note that the tropospheric thermally direct overturning circulation
 530 in this model is not meant to realistically mimic the Hadley circulation (Held and Hou 1980). Rather, its purpose in
 531 this model is to understand how tropopause geopotential anomalies associated with tropospheric
 532 circulations influence the stratospheric circulation.

534 What is the sensitivity of the stratospheric circulation to $\hat{\alpha}_{\text{rad}}$? Figure 6a,b shows the vertical
 535 profile of anomalous geopotential and vertical velocity, for varying values of $\hat{\alpha}_{\text{rad}}$. In all the solutions
 536 presented here, the tropospheric wave drag is fixed. We first observe that for all the solutions, the
 537 geopotential anomaly maximizes at the tropopause, and there is a significant barotropic geopotential
 538 component associated with all of the solutions. These positive geopotential anomalies decay as



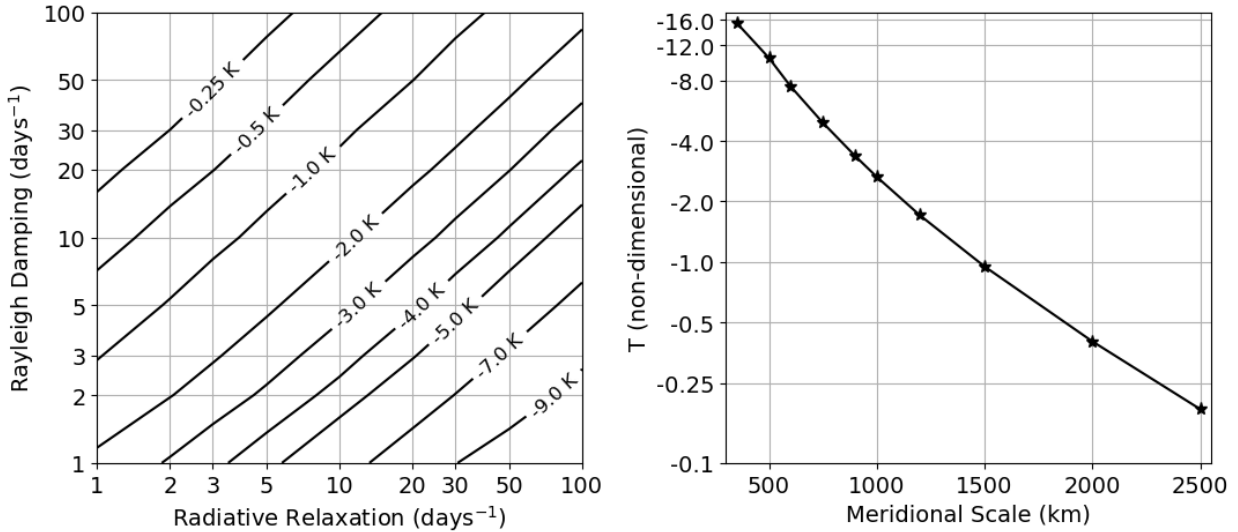
547 **FIG. 6.** (a) Vertical profiles of non-dimensional geopotential and (b) vertical velocity, at $y = 1.5$, for varying
 548 values of radiative relaxation, at a fixed Rayleigh damping (wave drag) of 25 days^{-1} . Dashed lines show the
 549 geopotential and vertical velocity associated with a pure baroclinic mode (normalized so that the peak vertical
 550 velocity is 0.02). (c), (d) are the same as (a), (b), respectively, except for varying values of stratospheric Rayleigh
 551 damping, at a fixed radiative relaxation rate of 25 days^{-1} . Tropopause is defined at 16-km, and tropospheric
 552 Rayleigh damping is fixed at 25 days^{-1} .

539 one moves upwards into the stratosphere, but the rate at which they decay is determined by the
 540 aforementioned parameters. When $\hat{\alpha}_{\text{rad}} = 1 \text{ day}^{-1}$, we observe a slow decay of the tropopause
 541 geopotential as one moves upwards into the stratosphere, and large upwelling values in the lower
 542 stratosphere. In contrast, when radiation is very slow ($\hat{\alpha}_{\text{rad}} = 100 \text{ day}^{-1}$), there is almost no
 543 penetration of the tropospheric vertical velocity into the stratosphere. This is associated with a
 544 tropospheric vertical velocity profile that is nearly entirely composed of the first baroclinic mode.
 545 As expected, radiative damping plays a large role in the communication of the tropopause forcing
 546 into the stratosphere.

553 The stratospheric response to a steady tropopause geopotential anomaly also shows a strong
554 dependence to \hat{D}_s . This is not surprising, given the criticality of wave-drag in the zonally-
555 symmetric solutions. Figure 6c,d shows the solutions with varying \hat{D}_s and a fixed radiative
556 damping time scale. The behavior of the coupled solutions are qualitatively similar to that inferred
557 from the isolated stratosphere solutions, in that faster wave-drag time scales increase the decay
558 of the tropopause geopotential into the stratosphere. In addition, faster wave-drag time scales are
559 associated with increased upwelling in the lower stratosphere, though the differences across the
560 parameters shown are smaller in magnitude than that when varying the radiative damping time
561 scale. This result could be a result of the simple relaxational form of wave-drag used in this study,
562 which does not capture detailed aspects of wave-forcing (Ming et al. 2016b). Regardless, the
563 numerical solutions confirm the mathematical analysis, in that both radiative damping and wave-
564 drag can modulate the stratospheric response to tropospheric forcing. Note, in a similar linear
565 system, PE99 found solutions to a stratosphere perturbed through tropospheric thermal forcing
566 that showed stratospheric upwelling nearly comparable in magnitude to that of the troposphere,
567 which was deemed as unrealistic. In PE99, the radiative relaxation time scale was 10 days^{-1} and
568 the relaxational wave-drag time scale was 500 days^{-1} , which corresponds to small ξ , and large
569 penetration of the tropospheric circulation into the stratosphere.

570 The vertical shape of the geopotential profiles above the tropopause also allows for an estimate of
571 the magnitude of the tropopause temperature cold anomaly as a function of tropospheric heating.
572 Figure 7, left, shows the temperature anomaly right above the tropopause, per degree of warming
573 in the boundary layer, as a function of the radiative damping and Rayleigh damping time scales.
574 In general, the longer the radiative damping time scales, the larger the temperature anomaly (as
575 pointed out by Randel et al. (2002)). In addition, there is also a strong dependence of the tropopause
576 temperature anomaly on the Rayleigh damping time scale: the faster the damping, the larger the
577 magnitude of the temperature anomaly. It is clear that both the magnitudes of the Rayleigh damping
578 (wave-drag) and radiative damping play significant roles in modulating the temperature anomaly
579 above the tropopause.

580 Interestingly, for “Earth-like” estimates of the time scale of Rayleigh damping and radiative
581 relaxation ($O(10)$ days $^{-1}$), the temperature anomalies just above the tropopause are around 2-3
582 times the magnitude of the boundary layer anomalies, slightly larger than what is observed in



588 FIG. 7. (Left): Temperature anomaly right above the tropopause, per degree of warming in the boundary
 589 layer, as a function of the radiative relaxation and Rayleigh damping (wave-drag) time scales. Rayleigh damping
 590 time scale is fixed in the troposphere and varied in the stratosphere. Both the abscissa and ordinate axes are
 591 in log-coordinates. (Right): Temperature anomaly right above the tropopause, per degree of warming in the
 592 boundary layer, as a function of the meridional length scale, L_y (km), for fixed Rayleigh damping and radiative
 593 relaxation. Ordinate axis is logarithmic.

583 convecting regions of the tropical atmosphere (see Fig. 5a in Holloway and Neelin (2007)). This
 584 theory thus provides a scaling argument for the degree of tropopause cooling that is expected per
 585 degree of boundary layer warming. Note that the derivative of the geopotential is discontinuous
 586 across the tropopause in this model, since we assume a instantaneous transition between quasi-
 587 equilibrium thermodynamics in the troposphere, and dry, passive dynamics in the stratosphere.

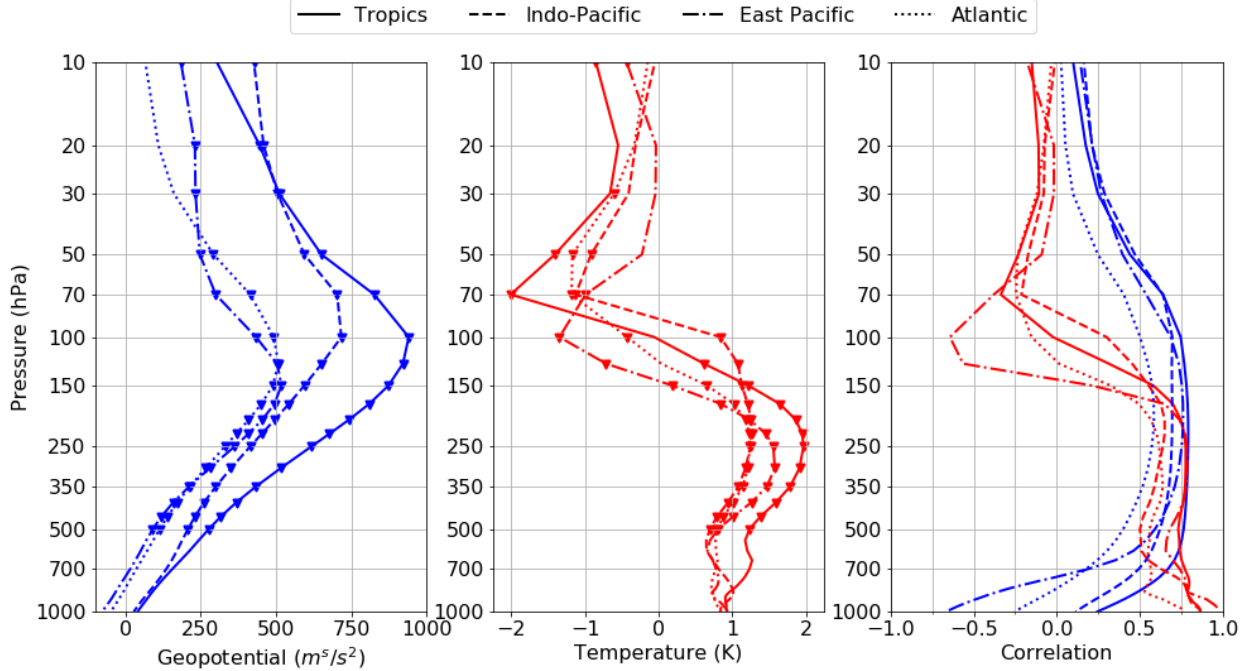
588 These theoretical results provide a potential explanation for the observed correlation between
 589 tropical-averaged SST anomalies and tropical stratospheric upwelling (Lin et al. 2015), as well
 590 as the anti-correlation between SST and tropopause temperature (Holloway and Neelin 2007).
 591 First, an SST anomaly is communicated throughout the depth of the troposphere through moist
 592 convection. Indeed, observations have found strong positive correlations between the tropopause
 593 geopotential anomaly and the boundary layer temperature anomaly (Holloway and Neelin 2007).
 594 The tropopause geopotential anomaly is initially associated with cold temperature anomalies just
 595 above the tropopause. The strength of radiative relaxation then determines the time scale at

602 which the geopotential anomaly rises in the stratosphere through diabatic heating. In the zonally-
603 symmetric case, the presence of wave-drag, through conservation of angular momentum, disrupts
604 this process and induces a meridional overturning circulation that mediates the vertical scale at
605 which the geopotential anomaly can rise in the stratosphere.

606 Our work shows that, at least in the zonally symmetric case, the ratio between the strength
607 of radiative relaxation and that of Rayleigh damping are significant factors in determining the
608 response of the stratosphere to an SST anomaly. However, there are a number of other quantities
609 unveiled through the non-dimensionalization that are also important. Surface friction, for instance,
610 factors into γ . In general, increasing the magnitude of F does little to change the behavior of
611 the stratospheric response to tropospheric forcing when ξ is large, since F only enters in γ and
612 $\xi\gamma$ is what matters for the tropopause boundary condition. The tropospheric & stratospheric
613 stratification, as well as the shape and length scale of the SST (or tropopause) perturbation (L_y),
614 also factor into the non-dimensional parameters that control the vertical decay scale of tropopause
615 geopotential anomalies. The horizontal scale of the SST anomaly can also be quite important, due
616 to the dependence of S on L_y^{-4} . Figure 7, right shows the dependence of the temperature anomaly
617 above the tropopause on L_y . There is an approximately logarithmic scaling of the temperature
618 anomaly with the meridional length scale of the tropopause anomaly, at least across the range of
619 L_y in the experiments. Correspondingly, the geopotential response in the stratosphere is muted
620 for small L_y (not shown). Thus, large horizontal scale tropospheric heating anomalies have a
621 larger penetrative depth into the stratosphere, but are also associated with smaller (in magnitude)
622 temperature anomalies at the tropopause.

623 4. Tropopause forcing in reanalysis data

624 In this section, we evaluate the proposed theory using the ERA5 re-analysis (Hersbach et al.
625 2019b,a). We use monthly fields of SST, geopotential, and temperature, over the years 1979-2022.
626 The Quasi-Biennial Oscillation (QBO) is regressed out of the geopotential and temperature fields,
627 by using the 50-hPa zonal wind averaged over the tropics. In particular, we will analyze correlations
628 between metrics of tropospheric warming and stratospheric cooling, on the global scale and the
629 local scale.



630 FIG. 8. (Left) Linear coefficient of geopotential at varying levels, regressed onto regionally-averaged SST
 631 anomalies. Above 500-hPa, significant correlations at the 1% level (two-sided) are denoted by upside-down
 632 triangles. (Middle) Same as the left panel but for temperature. (Right) Vertical dependence of the correlation
 633 coefficients for (blue) geopotential and (red) temperature. The regions are (solid) the entire tropics [20°S - 20°N],
 634 (dashed) the Indo-Pacific region [40°E-120°E], (dot-dashed) the East Pacific region [180°E-260°E], and (dotted)
 635 the Atlantic region [80°E-0°]. Vertical level is scaled as the logarithm of pressure.

636 To begin, we regress the anomalous tropical-averaged geopotential, at different vertical levels,
 637 onto the tropical-averaged SST anomaly. Anomalies are generated by subtracting the linear trend
 638 in each field, as well the seasonal cycle. Figure 8, solid lines, shows the coefficients of the linear
 639 regressions of geopotential and temperature onto SST. We first observe an approximate moist-
 640 adiabatic structure in the tropical tropospheric geopotential, consistent with quasi-equilibrium and
 641 the findings of previous studies (Holloway and Neelin 2007). We also see a large, significant
 642 correlation ($r \approx 0.75$) between tropical-averaged SST and the corresponding 100-hPa geopotential.
 643 The magnitude of the geopotential anomaly maximizes at 100-hPa, which is interpreted as an
 644 approximate tropopause level, since below this level there is warming, and above this level there
 645 is cooling (this is not exact, since the cold-point tropopause could occur above this level). Note

the similarity to the geopotential profile shown in Figure 6, which also maximizes around the climatological tropopause. This is indicative of a tropopause geopotential anomaly that is induced by an SST anomaly. The coefficient magnitudes and correlations decay with increasing height in the stratosphere, but are still statistically significant and non-negligible even at 20-hPa. Note, for a pure baroclinic mode anomaly, the surface geopotential would be anti-correlated with the upper troposphere anomaly (and the SST). Thus, when the surface geopotential is positively correlated with the upper tropospheric anomaly, there is significant barotropic component to the geopotential profile. We indeed observe that the tropical-averaged surface geopotential is positively correlated with both SST and the upper tropospheric geopotential, highlighting the role of the barotropic mode and the troposphere’s communication with the stratosphere.

The temperature structure of the tropical troposphere is also approximately moist-adiabatic, as also shown in Holloway and Neelin (2007). Figure 8 also shows that the tropics-averaged 70-hPa temperature is modestly but significantly anti-correlated ($r \approx -0.34$) with surface temperature. We also observe temperature anomalies at 70-hPa (lower stratosphere) to be approximately two times larger in magnitude than that of the surface, which is in agreement with the estimates shown in Figure 7. This is not exactly equivalent with the quantity derived in the left portion of Figure 7, as the regridded, pressure-interpolated output for ERA5 does not have many vertical levels near the tropopause, such that sharp reversals in the temperature response might be smoothed out. While data on the underlying model levels is available at a much higher vertical resolution, the ensuing analysis is very data intensive and left for future work.

The same relationships are also observed on regional scales (the Indo-Pacific, East Pacific, and the Atlantic), as shown in Figure 8. The geopotential anomalies maximize at 100-hPa in the Indo-Pacific, at 125-hPa in the Atlantic, and at 150-hPa in the East Pacific. Thus, the level at which the geopotential anomaly maximizes is influenced by the mean SST of the region (the East Pacific has the coldest climatological SSTs, while the Indo-Pacific has the warmest). In addition, the cold anomaly associated with SST warming maximizes above the level of maximum geopotential. The regional scale geopotential anomalies persist upwards to around 50-hPa, though the correlations drop significantly in magnitude, and the statistical significance ceases around 50-hPa. This means that regional and local scale variations in the lower stratospheric geopotential (50-hPa and 70-hPa) are strongly influenced by the tropopause geopotential in the same region. In general, the

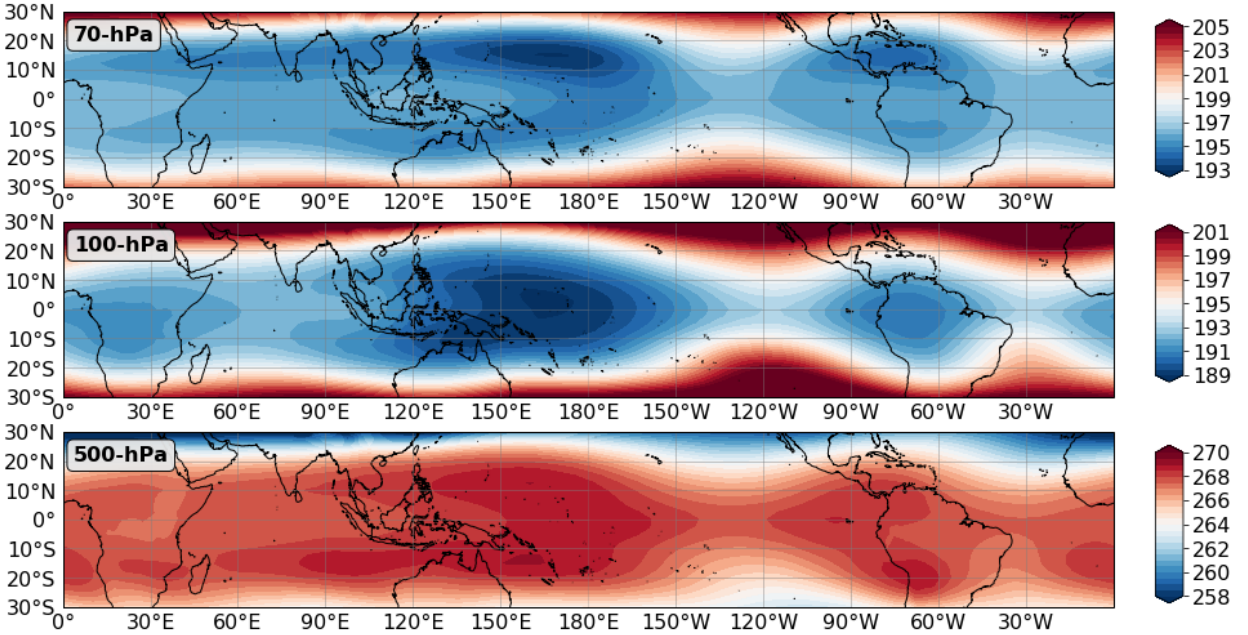
676 temperature anti-correlations are strongest in the East Pacific region – this may because there are
677 large SST perturbations in this region as a consequence of El Niño-Southern Oscillation variability,
678 increasing the signal of the relationship.

679 Of course, this analysis is not definitive proof that there is a quasi-balanced response of the
680 stratosphere to tropopause forcing. After all, if stratospheric temperature is modulated by tropical
681 heating through changes to wave-drag (Garcia and Randel 2008; Calvo et al. 2010; Lin et al. 2015),
682 then one would also expect the geopotential to decay with height in the stratosphere, as is shown in
683 Figure 8. Perhaps what would serve as stronger evidence for the processes described in this study
684 is if the spatial signature of tropospheric warming is retained in that of stratospheric cooling. If
685 true, this implies that lower stratospheric temperature is also influenced by “bottom-up” processes
686 (Garfinkel et al. 2013; Fu 2013) – not just “top-down” processes.

687 In the tropics, the surface temperature need not always be connected to tropospheric warming,
688 especially if the boundary layer moist static energy is lower than the saturation moist static energy
689 of the free troposphere. This is possible since temperature gradients in the tropical atmosphere are
690 weak, owing to the smallness of the Coriolis force, such that convecting regions more effectively
691 modulate the free tropospheric moist static energy (Sobel and Bretherton 2000). Thus, we use
692 500-hPa temperature as a proxy for local tropospheric warming.

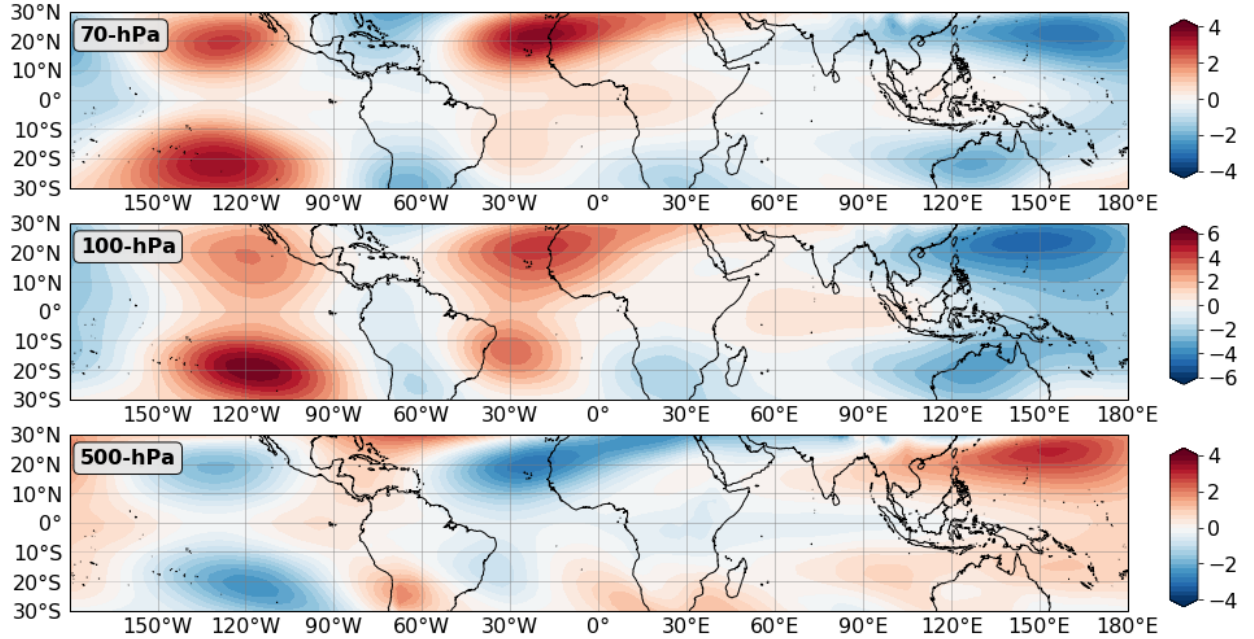
693 Figure 9 shows a map of the DJF-averaged 500-hPa climatological temperature , a proxy for
694 tropospheric heating, and the climatological temperature at 100- and 70-hPa in the lower strato-
695 sphere (these maps are well known and have been shown before, for instance in Dima and Wallace
696 (2007); Fueglistaler et al. (2009); Grise and Thompson (2013), but with different interpretations).
697 Here, we observe the warmest 500-hPa temepratures are in regions typically associated with active
698 convection (the West Pacific warm pool, equatorial South America, and equatorial Africa). Note
699 that tropospheric heating is a byproduct of convection. Furthermore, these same regions are where
700 the coldest 100-hPa and 70-hPa temperatures are also observed. Importantly, the coldest temper-
701 atures in the lower stratosphere occur right on or close to the equator, where the Coriolis force is
702 small. At 70-hPa, the signature of the equatorial 100-hPa cold anomalies disappears. This may be
703 a manifestation of the shallow vertical Rossby penetration depth of anomalies on the equator.

704 In order to further emphasize spatial variability, we compute monthly anomalies by subtracting the
705 climatological monthly zonal mean from the climatological monthly mean, and then average these



693 FIG. 9. DJF-averaged climatological temperature at (top) 70-hPa, (middle) 100-hPa, and (bottom) 500-hPa.
 694 Note the strong anti-correlation in tropospheric and lower stratospheric temperature.

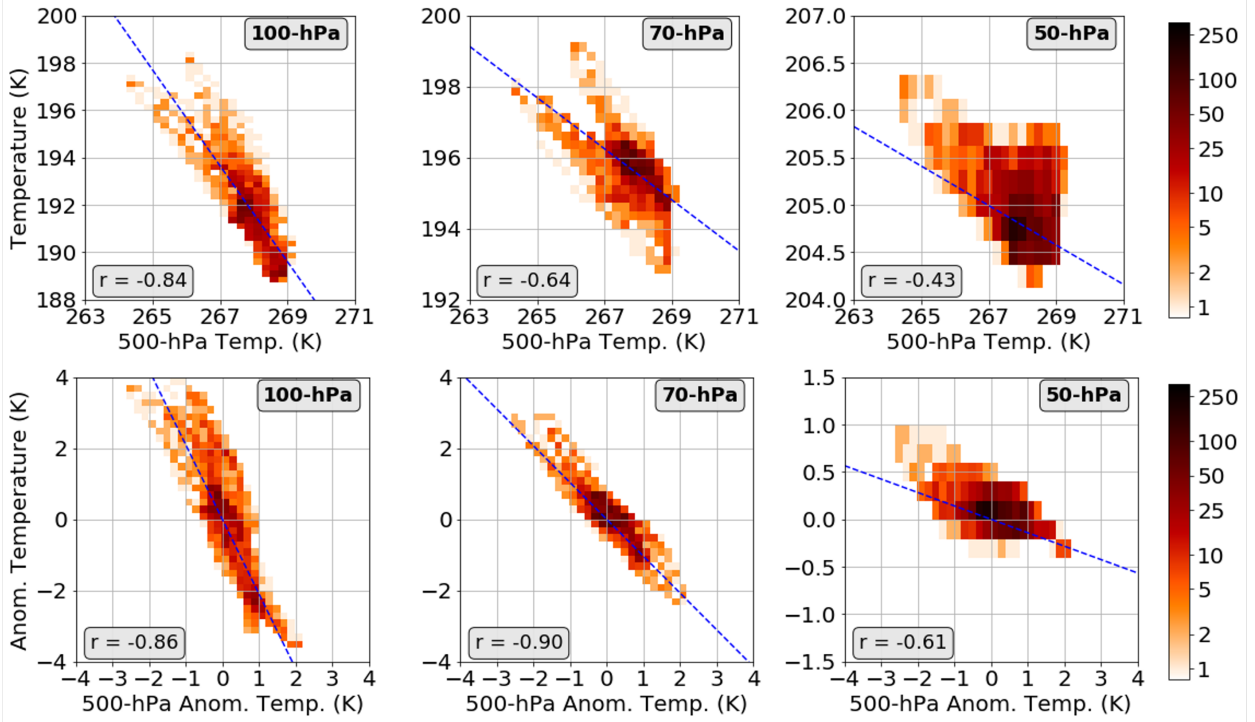
712 across December-January-February (DJF). Figure 10 shows maps of the DJF-averaged temperature
 713 anomalies at 500-, 100- and 70-hPa. Note the difference in the color scale at 100-hPa. It is evident
 714 that 500-hPa temperature is an excellent predictor of both the 100-hPa and 70-hPa temperature
 715 anomaly, though the strongest patterns are observed in the subtropical regions and associated with
 716 Rossby-wave-like features. Still, spatial variability in the tropospheric temperature anomaly is
 717 remarkably retained in the spatial variability of the stratospheric temperature. Furthermore, the
 718 lower-stratospheric temperature anomalies can be rather large (upwards to around 4 degrees in
 719 magnitude at 100-hPa and 70-hPa), though the total area encompassed by these large anomalies is
 720 small. There is also some qualitative evidence from the maps in Figure 10 that suggests that the
 721 magnitude of the lower stratospheric temperature anomalies is dependent on the horizontal scale
 722 of the tropospheric anomaly. For instance, from 60°W to 30°E in the Northern Hemisphere, there
 723 is a large-scale tropospheric cold anomaly of peak magnitude around 2 degrees. The associated
 724 temperature anomaly at 100-hPa is around 4 degrees. There is also a large-scale tropospheric warm
 725 anomaly of peak magnitude around 3 degrees in the Asian region (90°E to 180°E), with 100-hPa
 726 temperature anomalies of around -6 degrees. In contrast, smaller scale tropospheric anomalies



706 FIG. 10. DJF-averaged temperature anomaly at (top) 70-hPa, (middle) 100-hPa, (bottom) 500-hPa. Note
707 the strong anti-correlation in troposphere and lower stratospheric temperature. Anomalies are calculated by
708 subtracting the climatological monthly zonal mean, and averaging across the entire year. The color scale at
709 100-hPa is different than that at 70- and 500-hPa.

727 [(150°W to 90°W, 10°S to 30°S), (45°W to 15°W, 10°S to 25°S)] with comparatively weaker
728 peak temperature anomalies are associated with 100-hPa temperature anomalies that are of similar
729 magnitude to the 100-hPa temperature anomalies of the stronger, large scale anomalies. This is
730 in agreement with the proposed theory. In addition, at 70-hPa, the most prominent temperature
731 anomalies are those associated with the large-scale tropospheric anomalies (i.e. over the Northeast
732 African and Asian regions). This is also in agreement with the theory, in that the vertical depth
733 of the tropopause anomalies increases with the horizontal scale of the tropospheric anomaly. Of
734 course, the analysis here is mostly qualitative, and more substantial analysis is required to further
735 quantify the scale dependence of the lower stratospheric temperature anomalies, which will be
736 pursued in future work.

742 The remarkable correlation between tropospheric heating and stratospheric cooling can be further
743 quantified by regressions of 500-hPa temperature against lower-stratospheric temperature, among
744 all grid points shown in Figure 10. Figure 11, top-row, shows 2-D density histograms between the



737 FIG. 11. (Top-row) Grid-point 2D histograms between the 500-hPa climatological temperature and the (left)
738 100-hPa, (middle) 70-hPa and (right) 50-hPa climatological temperature, during DJF and from 15°S-15°N.
739 (Bottom-row) Same as top-row but for anomalous temperatures at each pressure level. Color scale is logarithmic,
740 and indicates the bin count. Linear regressions are plotted as the dashed blue lines, with correlation coefficients
741 shown on the lower left of each panel.

745 500-hPa climatological temperature and the 100-, 70-, and 50-hPa climatological temperature, as
746 well as the linear regressions. We have subsetted the latitudinal region in this analysis to 15°S-
747 15°N, in order to focus on the tropical regions. Per degree of warming at 500-hPa, the cooling
748 response is around 2.0 degrees at 100-hPa ($r = -0.84$), 0.72 degrees at 70-hPa ($r = -0.64$), and
749 0.21 degrees at 50-hPa ($r = -0.43$). The correlations are all significant, and generally decrease in
750 strength as one moves up further in the stratosphere. The linear regressions of 500-hPa anomalous
751 temperature against lower stratospheric anomalous temperature tell a similar story, as shown in
752 Figure 11, bottom-row. Per degree of anomalous 500-hPa temperature, there is a cooling response
753 of around 2.1 degrees at 100-hPa ($r = -0.86$), 1.03 degrees at 70-hPa ($r = -0.90$), and 0.14 degrees
754 at 50-hPa ($r = -0.61$). Note that while this paper focuses on the tropics, the proposed mechanism

755 need not only apply to the tropics (though Rossby wave excitation can be important outside of
756 the tropics). In fact, the correlations are even stronger if one extends the region of analysis to
757 30°S-30°N.

758 While the monthly anomalies shown in Figure 10 are averaged across DJF, there is significant
759 seasonal variability in the pattern of 500-hPa tropospheric temperature (not shown). The analysis
760 can be repeated by separating into various seasons, and we find that the local-scale anti-correlation
761 are generally strongest during boreal winter, and weakest during boreal summer (not shown). Still,
762 the results and interpretation remained unchanged: 500-hPa temperature is strongly anti-correlated
763 with lower stratospheric temperature. It is important to note that these correlations do not suggest
764 that there are correlations on significantly smaller horizontal scales; as suggested by Figure 10, the
765 correlations merely reflect the large-scale structure of the temperature anomalies.

766 Therefore, the observational data suggests that there might be a quasi-balanced response of
767 the stratosphere to tropospheric thermal forcing in the real world. However, there is reason to
768 remain cautious. As detailed in Section 2, separating the effect of the vertical propagation of
769 planetary waves from that of the quasi-balanced response of the stratosphere is nearly impossible
770 in observational data. While we restricted our analysis to 15°S-15°N, further insight into the
771 relative contribution of each proposed mechanism to the anti-correlation between tropospheric and
772 lower stratospheric temperature is left for future work.

773 5. Summary and discussion

774 In this work, we present theoretical evidence for how tropopause geopotential anomalies, gen-
775 erated through tropospheric thermal forcing, can modulate upwelling in the stratosphere. Using
776 a conceptual model based on the linearized QGPV equations, we show that tropospheric thermal
777 forcing can induce a tropopause geopotential anomaly, which subsequently elicits a quasi-balanced
778 response in the stratosphere. The tropopause anomalies initially have vertically shallow structures
779 scaled by the Rossby penetration depth (i.e. the fast adjustment of the stratosphere). Afterwards,
780 radiative relaxation in the stratosphere acts to increase the vertical penetration of these anomalies.
781 In the steady-state limit, where radiative equilibrium is again satisfied, the stratospheric PV be-
782 comes barotropic, though it takes on the order of years to be achieved. The solutions are akin to
783 those of Haynes et al. (1991), who found that the stratosphere becomes barotropic above the level

784 of forcing (in this case, the tropopause). This theory provides another potential explanation for why
785 cold stratospheric anomalies form above areas with local tropospheric warming. Despite the focus
786 on the tropics in this study, this proposed mechanism need not be confined to the tropics. However,
787 the excitation of planetary waves as a response to tropospheric heating, which was ignored for
788 simplicity in this study, ought to be taken into account. This will be the subject of future research.

789 We then formulate a zonally symmetric troposphere-stratosphere linear β -plane model, which
790 couples a convecting troposphere to a dry and passive stratosphere. We show that zonally-
791 symmetric tropospheric thermal forcing (via SST-anomalies) can directly force upwelling in the
792 lower stratosphere, provided the wave response is modeled purely as a response to the forced cir-
793 culation. The stratospheric response to tropospheric forcing is controlled by two non-dimensional
794 parameters: (1) ξ , a dynamical aspect ratio (Garcia 1987; Plumb and Eluszkiewicz 1999; Haynes
795 2005; Ming et al. 2016b), and (2) γ , a ratio between the stratospheric drag and tropospheric drag.
796 The main role of the tropospheric drag is to excite the tropospheric barotropic mode, which couples
797 the troposphere with the stratosphere. In the limit that the radiative relaxation is much stronger than
798 wave drag, the stratospheric response to a tropopause forcing asymptotically becomes barotropic,
799 while in the opposite limit, the vertical length scale of the tropopause forcing becomes extremely
800 small. We find that the stratospheric response to zonally-symmetric tropospheric forcing is largely
801 dependent on the radiative relaxation rate, the Rayleigh damping time scale of wave-drag, and the
802 horizontal scale. Our analyses show that the tropopause temperature anomaly is also modulated
803 by all of these quantities.

804 We also use reanalysis data to show that tropical and regionally averaged lower-stratospheric
805 temperatures are modestly and negatively correlated with SSTs in the same areas. In general, the
806 temperature anomalies per degree of warming in the boundary layer are approximately equivalent
807 to the corresponding theoretical predictions, at least when using "Earth-like" estimates of the time
808 scale of wave-drag and radiative relaxation. Furthermore, we show that the spatial variability in
809 lower-stratospheric temperature anomalies is strongly correlated with the spatial variability in 500-
810 hPa tropospheric temperatures. Significant correlations are seen upwards to 50-hPa, which suggests
811 that there is a quasi-balanced response of the stratospheric to tropospheric forcing. This provides
812 a scale-dependent theory for the oft-observed anti-correlation between tropospheric warming and

813 stratospheric cooling (Johnson and Kriete 1982; Gettelman et al. 2002; Holloway and Neelin 2007;
814 Kim and Son 2012; Virts and Wallace 2014; Kim et al. 2018).

815 The widely accepted theory of tropical stratospheric upwelling is that it is mechanically driven by
816 sub-tropical wave-drag (Haynes and McIntyre 1987; Plumb and Eluszkiewicz 1999). There is am-
817 ple evidence from numerical modeling suggesting that wave-dissipation is a dominant mechanism
818 that modulates mean and interannual upwelling in both the lower stratosphere and TTL (Boehm
819 and Lee 2003; Norton 2006; Calvo et al. 2010; Ryu and Lee 2010; Gerber 2012; Ortland and
820 Alexander 2014; Kim et al. 2016; Jucker and Gerber 2017, among many others). Of course, it is
821 theoretically impossible to have flow across angular momentum contours without some momentum
822 source. We emphasize that in no way does this work attempt to disprove the role sub-tropical wave
823 drag has in modulating tropical stratospheric upwelling. In this model, even though wave-drag acts
824 as a Rayleigh damping, as in the linear system described in PE99, it is an important modulator of
825 the upwelling response.

826 As shown in this study, the vertical penetration of the geopotential anomaly (and the rate at
827 which the stratospheric circulation crosses angular momentum surfaces) is strongly a function of
828 the wave drag. If the wave-drag is a function of the zonal mean state, which could vary in time
829 in part due to wave-forcing (Cohen et al. 2013; Ming et al. 2016b), then the vertical penetration
830 of the tropopause anomaly (and thus, its subsequent effect on upwelling) would also vary in time.
831 In this view, stratospheric wave-drag is, as countless studies have shown, a significant modulator
832 of tropical upwelling. However, wave drag alone may not suffice to explain certain features of the
833 behavior of the lower stratosphere, the foremost of which is the inverse correlation between SST
834 and lower stratospheric temperature anomalies, in both the zonal and meridional directions.

835 Our work, like PE99, investigates how tropospheric thermal forcing can modulate stratospheric
836 upwelling. In addition to mechanical and thermal forcing, this suggests a **third** way in which the
837 stratosphere can be forced – through the tropopause via tropospheric thermal forcing. In fact, the
838 theoretical analysis shown in PE99 finds that in the tropics, “the existence of a thermally driven
839 circulation and the breakdown of downward control go together” (if one accepts that what they
840 define as viscosity is representative of large-scale drag). However, their calculation of the linear
841 response to tropospheric thermal forcing exhibited large and unrealistic vertical penetration of
842 the tropospheric circulation into the stratosphere. This work shows that this is likely a result of

843 their assumptions of the strength of radiative relaxation ($\alpha_{\text{rad}} = 10 \text{ days}^{-1}$) and viscosity ($\hat{D} = 500$
844 days^{-1}). With $S = O(10^2)$, this is equivalent to $\xi \approx 3$. In this regime, our theory predicts extensive
845 penetration of the tropospheric circulation into the stratosphere, as in Figure 4 and 6.

846 In general, it is difficult to infer causality from diagnostic relations. For example, in the
847 Transformed-Eulerian Mean equations, it is not clear how much of the wave-drag is an exter-
848 nal forcing, as opposed to a response to a circulation that has a different forcing. Of course,
849 variations in wave-drag that are independent of those of the circulation support the idea that waves
850 can force the circulation. This aspect of the stratosphere has been well studied. But what if
851 wave-drag acted purely as a response to the circulation? (Note that these ideas are at opposite
852 ends of the spectrum with regards to the extent waves drive the circulation)? Then, at least in
853 our framework, the causality becomes very clear – SST forces the stratosphere by imposing a
854 tropopause geopotential anomaly. Of course, one could take the wave-drag term ($-D_s u_s$) and use
855 it to diagnose the associated upwelling response. However, that does not imply that waves are the
856 forcing mechanism of the circulation.

857 There are a few pieces of observational evidence that could be interpreted to be in favor of
858 the proposed theory. As stated earlier, the spatial variability of lower-stratospheric temperature
859 is strongly correlated with that of the troposphere, when considering both the climatological and
860 anomalous temperatures. In contrast, wave-drag, in its classical arguments, can only explain
861 departures of temperature from the zonal-mean (Andrews et al. 1987). This is by no means a small
862 feat, since the annual cycle in tropical-averaged temperature near the tropopause is around 8K,
863 around a factor of two larger than the peak temperature anomalies shown in Figure 10 (Chae and
864 Sherwood 2007).

865 However, the quasi-balanced response of the stratosphere to tropopause forcing could serve as
866 a potential explanation for a few outstanding issues. For instance, it can explain why there is
867 peak tropical upwelling on the summer-side equator (Rosenlof 1995). It could also help to explain
868 the observed connection between boundary layer temperature anomalies and lower stratospheric
869 temperature anomalies, as well as the high correlations between tropical SST and the upwelling
870 strength of the shallow BDC branch, which is observed on all time scales (Lin et al. 2015; Abalos
871 et al. 2021). Numerical modeling suggests that strengthening of the sub-tropical jets changes
872 the upward propagation of waves (Garcia and Randel 2008; Calvo et al. 2010; Shepherd and

873 McLandress 2011), ultimately strengthening the wave-driven stratospheric upwelling, although the
874 exact specifics seem to vary from model to model (Calvo et al. 2010; Simpson et al. 2011). In the
875 zonally symmetric coupled troposphere-stratosphere theory analyzed in this work, an equatorial
876 SST anomaly is not only associated with strengthening of the sub-tropical jets (which no doubt
877 could change the sub-tropical distribution of wave-drag in the real-world), but also a strengthening
878 of the tropopause geopotential. As such, the theory proposed in this work does not have to be
879 mutually exclusive with those based on wave-drag.

880 Besides the inclusion of a relaxational wave-drag (shown to be a poor assumption), our work stays
881 silent on how the momentum budget must change in order to balance changes in the meridional
882 circulation (Ming et al. 2016b). However, there would undoubtedly be a large scale wave response to
883 steady tropospheric heating (Gill 1980). Thus, disentangling the effects of heating from the ensuing
884 wave-response is quite complicated, as the two occur in concert. While other studies have analyzed
885 the wave-response to tropospheric heating (Ortland and Alexander 2014; Jucker and Gerber 2017)
886 (as well as its subsequent effects on the stratospheric circulation), we have instead focused on the
887 **steady** response to tropospheric heating. In general, however, when tropical tropospheric heating
888 is used to generate a wave response, it is difficult to separate the tropopause forcing mechanism
889 described in this study from wave driving. For instance, Jucker and Gerber (2017) used idealized
890 GCM simulations to show that the inclusion of a tropical warm pool significantly changed the
891 annual-mean temperature of the tropical tropopause (and more importantly, more so than mid-
892 latitude land-sea contrast and orographic forcing). However, the imposition of a warm pool will
893 both intensify the tropopause anti-cyclone over the region, and trigger a large-scale wave response.
894 According to the analysis shown in this study, the increased tropopause geopotential will act to
895 cool the tropopause and induce more upwelling (as would increased wave-drag from the large-scale
896 wave response). Separately, Ortland and Alexander (2014) forced equatorial waves by prescribing
897 time-varying latent heating anomalies in a primitive equation model, and found that stationary
898 waves and weakly westward propagating waves are most responsible for driving residual-mean
899 upwelling in the TTL. Again, tropospheric heating will induce a tropopause geopotential anomaly,
900 such that the steady tropospheric forcing is not separated from the wave response. Regardless,
901 both of the modeling results in Ortland and Alexander (2014) and Jucker and Gerber (2017) show

902 that at least in numerical models, the seasonal cycle in upwelling in the tropical tropopause layer
903 cannot be explained by tropospheric thermal forcing.

904 It is only fair for these conclusions to be discussed alongside the assumptions posited in this
905 model. In this model, we assume that there is an instantaneous transition between tropospheric,
906 quasi-equilibrium dynamics, and passive, dry stratospheric dynamics. In reality, the presence of
907 the TTL could dampen the upwards influence of tropospheric forcing. The assumption of a moist
908 adiabatic lapse rate all the way to the tropopause is one that is has mixed observational evidence,
909 which suggests that the free tropospheric temperature anomalies, per degree of warming in the
910 boundary layer, approximately follow a moist adiabat up to around 200-hPa, after which temperature
911 anomalies transition to being out of phase with lower tropospheric temperature anomalies [see
912 Figure 8 and Holloway and Neelin (2007)] (though some of this may be owing to time averaging
913 with a vertically moving tropopause). While the proposed theory can predict the magnitude of the
914 tropopause temperature anomalies with respect to boundary layer warming, it does not include a
915 transition layer. The presence of a transition layer could, in theory, dampen the vertical penetration
916 of thermal forcing in the troposphere. This will be the subject of future research.

917 Finally, we also assume a fixed tropopause height that interfaces the two regimes, as in PE99. This
918 makes the analysis mathematically tractable. Indeed, one would expect tropospheric temperature to
919 affect tropopause height (Held 1982; Lin et al. 2017). The relaxation of both of these assumptions
920 will be the subject of future research, but requires a theory for how moist convection interacts with
921 the transition layer. More research is necessary to understand the role of convection in modulating
922 the behavior of the transition layer.

923 The analysis carried out in section 4 uses the ERA5 reanalysis dataset, which is not truly obser-
924 vational data. This could be mitigated by the use of GPS radio-occultation (RO) measurements,
925 provided by the COSMIC mission (Anthes et al. 2008). The high vertical resolution of GPS-RO
926 measurements could be leveraged in future work, as done in Grise and Thompson (2013). Further-
927 more, while we focused on large-scale tropospheric anomalies in this work, there are also numerous
928 mesoscale convective systems, usually with anticyclones at their tops, that might also be able to
929 contribute to tracer transport into the stratosphere. Higher resolution observational data, such as
930 that provided by GPS RO measurements, could also be useful to evaluate this possibility.

931 *Acknowledgments.* The author thanks Adam Sobel and Peter Hitchcock for comments and sug-
 932 gestions on earlier versions of this work. The authors also thank two anonymous reviewers and
 933 Peter Haynes for their helpful suggestions, which greatly improved the manuscript. In particular,
 934 the authors are grateful for Peter Haynes’s suggestions on the formulation of the coupled boundary
 935 condition. J. Lin gratefully acknowledges the support of the National Science Foundation through
 936 the NSF-AGS Postdoctoral Fellowship, under award number AGS-PRF-2201441.

937 *Data availability statement.* The monthly-mean ERA5 data for sea-surface tem-
 938 perature is available at <https://cds.climate.copernicus.eu/cdsapp#!/dataset/reanalysis-era5-single-levels-monthly-means> via DOI: 10.24381/cds.f17050d7 Hers-
 939 bach et al. (2019b). The monthly-averaged ERA5 data for temperature and
 940 geopotential are available at <https://cds.climate.copernicus.eu/cdsapp#!/dataset/reanalysis-era5-pressure-levels-monthly-means> via DOI: 10.24381/cds.6860a573
 941 Hersbach et al. (2019a). All code to generate the data from the theoretical models are avail-
 942 able at https://github.com/linjonathan/steady_coupled_trop_strat.
 943

945 APPENDIX

946 Details on Solutions

947 *a. Solutions to Conceptual Model in Section 2*

948 The general solution to the homogeneous version of Eq. 9 ($q(z) = 0$) is:

$$949 G(z) = A \exp(m_+ z) + B \exp(m_- z) \quad (A1)$$

949 where $m_{\pm} = \frac{1 \pm \sqrt{1+4(k^2+l^2)}}{2}$. Note, since $k^2 + l^2 > 0$, $m_+ > 0$ and $m_- < 0$ for all $k > 0$ and $l > 0$. We
 950 next define the Green’s function, which satisfies

$$951 LG(z, \lambda) = \delta(z - \lambda) \quad (A2)$$

951 and is

$$G(z, \lambda) = \begin{cases} A \exp(m_+ z) + B \exp(m_- z), & \text{for } 0 < z < \lambda \\ C \exp(m_+ z) + D \exp(m_- z), & \text{for } \lambda < z < z_{\text{top}} \end{cases} \quad (\text{A3})$$

952 where z_{top} is assumed to be the top of the domain. The lower boundary condition requires that:

$$A + B = \phi_T \quad (\text{A4})$$

953 and the upper boundary condition requires that:

$$C m_+ \exp(m_+ z_{\text{top}}) + D m_- \exp(m_- z_{\text{top}}) = 0 \quad (\text{A5})$$

954 Note that we choose to explicitly include z_{top} in Eq. A5, since numerically evaluating the Green's
955 functions requires $z_{\text{top}} < \infty$. Continuity of G across λ requires:

$$A \exp(m_+ \lambda) + B \exp(m_- \lambda) = C \exp(m_+ \lambda) + D \exp(m_- \lambda) \quad (\text{A6})$$

$$\lim_{\epsilon \rightarrow 0} \frac{\partial G}{\partial z} \Big|_{z=\lambda-\epsilon}^{z=\lambda+\epsilon} - \lim_{\epsilon \rightarrow 0} G \Big|_{z=\lambda-\epsilon}^{z=\lambda+\epsilon} = 1 \quad (\text{A7})$$

956 Eqs. A4-A7 are solved to obtain:

$$A = \frac{\phi_T - \frac{1}{m_d} (\exp(-m_- \lambda) - \frac{m_+}{m_-} \exp(-m_+ \lambda + m_d z_{\text{top}}))}{1 - \frac{m_+}{m_-} \exp(m_d z_{\text{top}})} \quad (\text{A8})$$

957 where

$$m_d = m_+ - m_- = \sqrt{1 + 4(k^2 + l^2)} > 0 \quad (\text{A9})$$

958 B, C , and D are then obtained using Eqs. A4, A5, and A6.

959 The Green's function can be convoluted with the source term (q) to obtain the geopotential:

$$\phi(z) = \int_0^\infty G(z, \lambda) q(\lambda) d\lambda \quad (\text{A10})$$

960 *b. Numerical Solver for Coupled Troposphere-Stratosphere*

961 In this section, we elaborate on the numerical solver of the coupled troposphere-stratosphere
962 system (Eq. 35, 46), given forcing in s^* . We approximate the meridional and vertical derivatives
963 with second-order and sixth-order central finite differences, respectively. Since our specified s^*
964 forcing is equatorially symmetric, we only have to discretize y from equator to pole, and impose
965 a Neumann boundary condition at the equator. However, y appears in the denominator in both
966 Eq. 35 and 46). We circumvent this issue by numerically evaluating the equator at $\epsilon = 10^{-5}$ (three
967 orders of magnitude smaller than the meridional grid spacing). y is evenly discretized from y_{\max}
968 to ϵ , where $y_{\max} = -10$. z is evenly discretized from the tropopause ($z^* = 1$) to the domain top,
969 $z_{\text{top}}^* = 7$. The boundary conditions are:

$$\phi(y = y_{\max}, z^*) = 0 \quad (\text{A11})$$

$$\frac{\partial \phi}{\partial y}(y = \epsilon, z^*) = 0 \quad (\text{A12})$$

$$\frac{\partial \phi}{\partial z}(y, z^* = z_{\text{top}}^*) = 0 \quad (\text{A13})$$

970 as well as the aforementioned Eq. 46 on the boundary $z^* = 1$. The solutions are ensured to solve
971 the original linear system of equations, as well as the boundary conditions, within numerical error.
972 Finally, we use the *findiff* Python package to solve the system numerically (Baer 2018).

973 **References**

974 Abalos, M., and Coauthors, 2021: The Brewer–Dobson circulation in CMIP6. *Atmospheric Chemistry*
975 and Physics, **21** (17), 13 571–13 591.

976 Andrews, D. G., J. R. Holton, and C. B. Leovy, 1987: *Middle atmosphere dynamics*. 40, Academic
977 press.

978 Anthes, R. A., and Coauthors, 2008: The COSMIC/FORMOSAT-3 mission: Early results. *Bull.*
979 *Amer. Meteor. Soc.*, **89** (3), 313–334.

980 Baer, M., 2018: *findiff* software package. URL <https://github.com/maroba/findiff>, <https://github.com/maroba/findiff>.

982 Birner, T., and H. Bönisch, 2011: Residual circulation trajectories and transit times into the
983 extratropical lowermost stratosphere. *Atmospheric Chemistry and Physics*, **11** (2), 817–827.

984 Boehm, M. T., and S. Lee, 2003: The implications of tropical Rossby waves for tropical tropopause
985 cirrus formation and for the equatorial upwelling of the Brewer–Dobson circulation. *J. Atmos.*
986 *Sci.*, **60** (2), 247–261.

987 Butchart, N., 2014: The Brewer–Dobson circulation. *Rev. Geophys.*, **52** (2), 157–184.

988 Calvo, N., R. Garcia, W. Randel, and D. Marsh, 2010: Dynamical mechanism for the increase in
989 tropical upwelling in the lowermost tropical stratosphere during warm ENSO events. *J. Atmos.*
990 *Sci.*, **67** (7), 2331–2340.

991 Chae, J. H., and S. C. Sherwood, 2007: Annual temperature cycle of the tropical tropopause: A
992 simple model study. *J. Geophys. Res. Atmos.*, **112** (D19).

993 Cohen, N. Y., E. P. Gerber, and O. Böhler, 2013: Compensation between resolved and unresolved
994 wave driving in the stratosphere: Implications for downward control. *J. Atmos. Sci.*, **70** (12),
995 3780–3798.

996 Danielsen, E. F., 1982: A dehydration mechanism for the stratosphere. *Geophys. Res. Lett.*, **9** (6),
997 605–608.

998 Dima, I. M., and J. M. Wallace, 2007: Structure of the annual-mean equatorial planetary waves in
999 the ERA-40 reanalyses. *J. Atmos. Sci.*, **64** (8), 2862–2880.

1000 Dobson, G. M. B., 1956: Origin and distribution of the polyatomic molecules in the atmosphere.
1001 *Proceedings of the Royal Society of London. Series A. Mathematical and Physical Sciences*,
1002 **236** (1205), 187–193.

1003 Emanuel, K. A., 1987: An air-sea interaction model of intraseasonal oscillations in the tropics. *J.*
1004 *Atmos. Sci.*, **44** (16), 2324–2340.

1005 Emanuel, K. A., 1994: *Atmospheric convection*. Oxford University Press, USA.

1006 Emanuel, K. A., J. David Neelin, and C. S. Bretherton, 1994: On large-scale circulations in
1007 convecting atmospheres. *Quart. J. Roy. Meteor. Soc.*, **120** (519), 1111–1143.

1008 Fu, Q., 2013: Bottom up in the tropics. *Nature Climate Change*, **3** (11), 957–958.

1009 Fu, Q., C. M. Johanson, J. M. Wallace, and T. Reichler, 2006: Enhanced mid-latitude tropospheric
1010 warming in satellite measurements. *Science*, **312** (5777), 1179–1179.

1011 Fueglistaler, S., M. Bonazzola, P. Haynes, and T. Peter, 2005: Stratospheric water vapor predicted
1012 from the Lagrangian temperature history of air entering the stratosphere in the tropics. *J.
1013 Geophys. Res. Atmos.*, **110** (D8).

1014 Fueglistaler, S., A. Dessler, T. Dunkerton, I. Folkins, Q. Fu, and P. W. Mote, 2009: Tropical
1015 tropopause layer. *Rev. Geophys.*, **47** (1).

1016 Garcia, R. R., 1987: On the mean meridional circulation of the middle atmosphere. *J. Atmos. Sci.*,
1017 **44** (24), 3599–3609.

1018 Garcia, R. R., and W. J. Randel, 2008: Acceleration of the Brewer–Dobson circulation due to
1019 increases in greenhouse gases. *J. Atmos. Sci.*, **65** (8), 2731–2739.

1020 Garfinkel, C., D. Waugh, L. Oman, L. Wang, and M. Hurwitz, 2013: Temperature trends in the
1021 tropical upper troposphere and lower stratosphere: Connections with sea surface temperatures
1022 and implications for water vapor and ozone. *J. Geophys. Res. Atmos.*, **118** (17), 9658–9672.

1023 Garny, H., M. Dameris, W. Randel, G. E. Bodeker, and R. Deckert, 2011: Dynamically forced
1024 increase of tropical upwelling in the lower stratosphere. *J. Atmos. Sci.*, **68** (6), 1214–1233.

1025 Gerber, E. P., 2012: Stratospheric versus tropospheric control of the strength and structure of the
1026 Brewer–Dobson circulation. *J. Atmos. Sci.*, **69** (9), 2857–2877.

1027 Gettelman, A., M. Salby, and F. Sassi, 2002: Distribution and influence of convection in the
1028 tropical tropopause region. *J. Geophys. Res. Atmos.*, **107** (D10), ACL–6.

1029 Gill, A. E., 1980: Some simple solutions for heat-induced tropical circulation. *Quart. J. Roy.
1030 Meteor. Soc.*, **106** (449), 447–462.

1031 Grise, K. M., and D. W. Thompson, 2013: On the signatures of equatorial and extratropical wave
1032 forcing in tropical tropopause layer temperatures. *J. Atmos. Sci.*, **70** (4), 1084–1102.

1033 Haynes, P., 2005: Stratospheric dynamics. *Annu. Rev. Fluid Mech.*, **37**, 263–293.

1034 Haynes, P., M. McIntyre, T. Shepherd, C. Marks, and K. P. Shine, 1991: On the "downward
1035 control" of extratropical diabatic circulations by eddy-induced mean zonal forces. *J. Atmos. Sci.*,
1036 **48** (4), 651–678.

1037 Haynes, P., and W. Ward, 1993: The effect of realistic radiative transfer on potential vorticity
1038 structures, including the influence of background shear and strain. *J. Atmos. Sci.*, **50** (20),
1039 3431–3453.

1040 Haynes, P. H., and M. E. McIntyre, 1987: On the evolution of vorticity and potential vorticity in
1041 the presence of diabatic heating and frictional or other forces. *J. Atmos. Sci.*, **44** (5), 828–841.

1042 Held, I. M., 1982: On the height of the tropopause and the static stability of the troposphere. *J.*
1043 *Atmos. Sci.*, **39** (2), 412–417.

1044 Held, I. M., and A. Y. Hou, 1980: Nonlinear axially symmetric circulations in a nearly inviscid
1045 atmosphere. *J. Atmos. Sci.*, **37** (3), 515–533.

1046 Hersbach, H., and Coauthors, 2019a: ERA5 monthly averaged data on pressure levels from 1979
1047 to present. *Copernicus Climate Change Service (C3S) Climate Data Store (CDS)*.

1048 Hersbach, H., and Coauthors, 2019b: ERA5 monthly averaged data on single levels from 1979 to
1049 present. *Copernicus Climate Change Service (C3S) Climate Data Store (CDS)*.

1050 Hitchcock, P., T. G. Shepherd, and S. Yoden, 2010: On the approximation of local and linear
1051 radiative damping in the middle atmosphere. *J. Atmos. Sci.*, **67** (6), 2070–2085.

1052 Holloway, C. E., and J. D. Neelin, 2007: The convective cold top and quasi equilibrium. *J. Atmos.*
1053 *Sci.*, **64** (5), 1467–1487.

1054 Holton, J. R., P. H. Haynes, M. E. McIntyre, A. R. Douglass, R. B. Rood, and L. Pfister, 1995:
1055 Stratosphere-troposphere exchange. *Rev. Geophys.*, **33** (4), 403–439.

1056 Jensen, E., and L. Pfister, 2004: Transport and freeze-drying in the tropical tropopause layer. *J.*
1057 *Geophys. Res. Atmos.*, **109** (D2).

1058 Johnson, R. H., and D. C. Kriete, 1982: Thermodynamic and circulation characteristics, of winter
1059 monsoon tropical mesoscale convection. *Mon. Wea. Rev.*, **110** (12), 1898–1911.

1060 Jucker, M., and E. Gerber, 2017: Untangling the annual cycle of the tropical tropopause layer with
1061 an idealized moist model. *J. Climate*, **30** (18), 7339–7358.

1062 Kerr-Munslow, A., and W. Norton, 2006: Tropical wave driving of the annual cycle in tropical
1063 tropopause temperatures. part I: ECMWF analyses. *J. Atmos. Sci.*, **63** (5), 1410–1419.

1064 Kiladis, G., K. Straub, G. Reid, and K. Gage, 2001: Aspects of interannual and intraseasonal
1065 variability of the tropopause and lower stratosphere. *Quart. J. Roy. Meteor. Soc.*, **127** (576),
1066 1961–1983.

1067 Kim, J., W. J. Randel, and T. Birner, 2018: Convectively driven tropopause-level cooling and its
1068 influences on stratospheric moisture. *J. Geophys. Res. Atmos.*, **123** (1), 590–606.

1069 Kim, J., W. J. Randel, T. Birner, and M. Abalos, 2016: Spectrum of wave forcing associated with
1070 the annual cycle of upwelling at the tropical tropopause. *J. Atmos. Sci.*, **73** (2), 855–868.

1071 Kim, J., and S.-W. Son, 2012: Tropical cold-point tropopause: Climatology, seasonal cycle,
1072 and intraseasonal variability derived from COSMIC GPS radio occultation measurements. *J.*
1073 *Climate*, **25** (15), 5343–5360.

1074 Kuang, Z., and C. S. Bretherton, 2004: Convective influence on the heat balance of the tropical
1075 tropopause layer: A cloud-resolving model study. *J. Atmos. Sci.*, **61** (23), 2919–2927.

1076 Lin, J., and K. Emanuel, 2022: On the effect of surface friction and upward radiation of energy on
1077 equatorial waves. *J. Atmos. Sci.*, **79** (3), 837–857.

1078 Lin, P., Y. Ming, and V. Ramaswamy, 2015: Tropical climate change control of the lower strato-
1079 spheric circulation. *Geophys. Res. Lett.*, **42** (3), 941–948.

1080 Lin, P., D. Paynter, Y. Ming, and V. Ramaswamy, 2017: Changes of the tropical tropopause layer
1081 under global warming. *J. Climate*, **30** (4), 1245–1258.

1082 Ming, A., P. Hitchcock, and P. Haynes, 2016a: The double peak in upwelling and heating in the
1083 tropical lower stratosphere. *J. Atmos. Sci.*, **73** (5), 1889–1901.

1084 Ming, A., P. Hitchcock, and P. Haynes, 2016b: The response of the lower stratosphere to zonally
1085 symmetric thermal and mechanical forcing. *J. Atmos. Sci.*, **73** (5), 1903–1922.

1086 Norton, W., 2006: Tropical wave driving of the annual cycle in tropical tropopause temperatures.
1087 part II: Model results. *J. Atmos. Sci.*, **63** (5), 1420–1431.

1088 Orbe, C., and Coauthors, 2020: GISS Model E2. 2: A climate model optimized for the middle at-
1089 mosphere—2. validation of large-scale transport and evaluation of climate response. *J. Geophys.*
1090 *Res. Atmos.*, **125** (24), e2020JD033 151.

1091 Ortland, D. A., and M. J. Alexander, 2014: The residual-mean circulation in the tropical tropopause
1092 layer driven by tropical waves. *J. Atmos. Sci.*, **71** (4), 1305–1322.

1093 Plumb, R. A., 2002: Stratospheric transport. *Journal of the Meteorological Society of Japan. Ser.*
1094 *II*, **80** (4B), 793–809.

1095 Plumb, R. A., and J. Eluszkiewicz, 1999: The Brewer–Dobson circulation: Dynamics of the
1096 tropical upwelling. *J. Atmos. Sci.*, **56** (6), 868–890.

1097 Randel, W., and M. Park, 2019: Diagnosing observed stratospheric water vapor relationships to
1098 the cold point tropical tropopause. *J. Geophys. Res. Atmos.*, **124** (13), 7018–7033.

1099 Randel, W. J., R. Garcia, and F. Wu, 2008: Dynamical balances and tropical stratospheric up-
1100 welling. *J. Atmos. Sci.*, **65** (11), 3584–3595.

1101 Randel, W. J., R. R. Garcia, N. Calvo, and D. Marsh, 2009: ENSO influence on zonal mean
1102 temperature and ozone in the tropical lower stratosphere. *Geophys. Res. Lett.*, **36** (15).

1103 Randel, W. J., R. R. Garcia, and F. Wu, 2002: Time-dependent upwelling in the tropical lower
1104 stratosphere estimated from the zonal-mean momentum budget. *J. Atmos. Sci.*, **59** (13), 2141–
1105 2152.

1106 Randel, W. J., F. Wu, and W. Rivera Ríos, 2003: Thermal variability of the tropical tropopause
1107 region derived from GPS/MET observations. *J. Geophys. Res. Atmos.*, **108** (D1), ACL–7.

1108 Randel, W. J., F. Wu, H. Voemel, G. E. Nedoluha, and P. Forster, 2006: Decreases in stratospheric
1109 water vapor after 2001: Links to changes in the tropical tropopause and the Brewer–Dobson
1110 circulation. *J. Geophys. Res. Atmos.*, **111** (D12).

1111 Rosenlof, K. H., 1995: Seasonal cycle of the residual mean meridional circulation in the strato-
1112 sphere. *J. Geophys. Res. Atmos.*, **100** (D3), 5173–5191.

1113 Ryu, J.-H., and S. Lee, 2010: Effect of tropical waves on the tropical tropopause transition layer
1114 upwelling. *J. Atmos. Sci.*, **67** (10), 3130–3148.

1115 Seviour, W. J., N. Butchart, and S. C. Hardiman, 2012: The Brewer–Dobson circulation inferred
1116 from ERA-Interim. *Quart. J. Roy. Meteor. Soc.*, **138** (665), 878–888.

1117 Shepherd, T. G., and C. McLandress, 2011: A robust mechanism for strengthening of the Brewer–
1118 Dobson circulation in response to climate change: Critical-layer control of subtropical wave
1119 breaking. *J. Atmos. Sci.*, **68** (4), 784–797.

1120 Sherwood, S. C., 2000: A stratospheric “drain” over the maritime continent. *Geophys. Res. Lett.*,
1121 **27** (5), 677–680.

1122 Simpson, I. R., T. G. Shepherd, and M. Sigmond, 2011: Dynamics of the lower stratospheric
1123 circulation response to ENSO. *J. Atmos. Sci.*, **68** (11), 2537–2556.

1124 Sobel, A. H., and C. S. Bretherton, 2000: Modeling tropical precipitation in a single column. *J.*
1125 *Climate*, **13** (24), 4378–4392.

1126 Taguchi, M., 2009: Wave driving in the tropical lower stratosphere as simulated by waccm. part i:
1127 Annual cycle. *J. Atmos. Sci.*, **66** (7), 2029–2043.

1128 Vallis, G. K., 2017: *Atmospheric and Oceanic Fluid Dynamics*. Cambridge University Press.

1129 Virts, K. S., and J. M. Wallace, 2014: Observations of temperature, wind, cirrus, and trace gases
1130 in the tropical tropopause transition layer during the MJO. *J. Atmos. Sci.*, **71** (3), 1143–1157.

1131 Yulaeva, E., J. R. Holton, and J. M. Wallace, 1994: On the cause of the annual cycle in tropical
1132 lower-stratospheric temperatures. *J. Atmos. Sci.*, **51** (2), 169–174.